Analysis of the Magnetocaloric Effect in Powder Samples Obtained by Ball Milling

J. S. Blázquez, L. M. Moreno-Ramírez, J. J. Ipus, V. Franco, A. Conde

University of Sevilla (SPAIN)

Sevilla, December 11th 2015

Scope of the talk

- Introduction to ball milling
- Approach to the dynamics of planetary ball mill
  - ✓An equivalent time approach
- Microstructure of ball milled powders
  - ✓Two scales: micro and nano
  - ✓Compositional homogenization
- Magnetic properties of ball milled powders
  - ✓Two regimes in the milling time dependence of magnetic anisotropy
  - ✓Factors affecting magnetic measurements in ball milled powders
  - ✓Magnetocaloric effect in ball milled powders
- Conclusions

Ball milling

- Large balls of a hard material impact on small powder particles.
- Competing mechanisms of fracture and cold welding yield powder particle size.
- Mechanical energy transferred to the powder trapped during collisions typically leads to crystal size reduction and, in some cases, to amorphization.

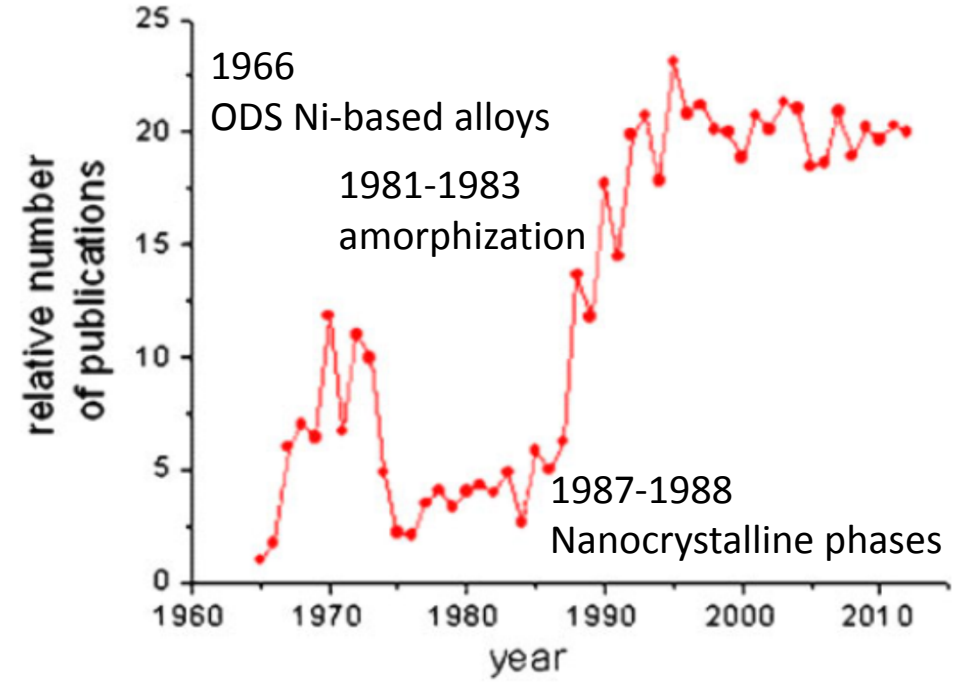

Fig. 1. Data obtained from Web of Science database. Results searching "mechanical alloy*" OR "ball mil*" as topic divided by results searching "material*" and normalized to the corresponding value in 1965.

Blázquez et al. JOM 65(2013)870

Different types of ball mills

Planetary

Shaker (SPEX)

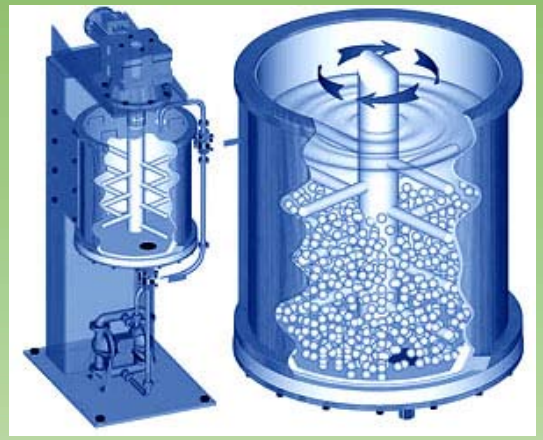

Attritor

Mainly friction

Mainly collisions

Large number of parameters involved

- Type of mill
- Milling speed (selected frequency)
  - ✓ Fixed in some mills. Relation between planetary and other mills
- Milling time
- Ball to powder weight ratio
- Extent of filling the vial
- Milling media (container and balls)
  - ✓ Prevent undesired contamination (tempered or hardened steel, tungsten carbide, silicon nitride, corundum, agate…)
  - ✓ Beware of impurities (e.g. 6 % Co in tungsten-carbide! or traces of Fe_2O_3 in agate)
- Milling atmosphere
  - ✓ Reactive milling, mechanochemical syntesis
- Process control agents
  - ✓ Surfactants reduce cold welding phenomenon
- Temperature of milling
  - ✓ Cryomilling (reduce cold welding phenomenon)

Approach to dynamics of planetary ball mill: An equivalent time approach

Sevilla, December 11th 2015

Schematic view of planetary mill

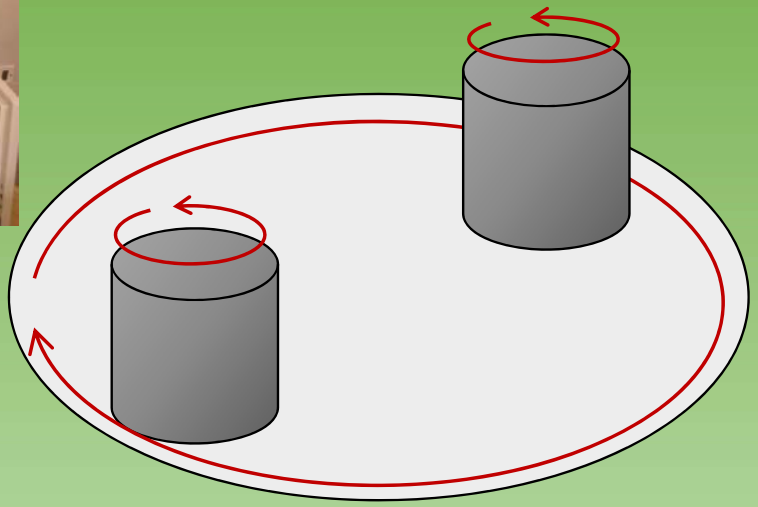

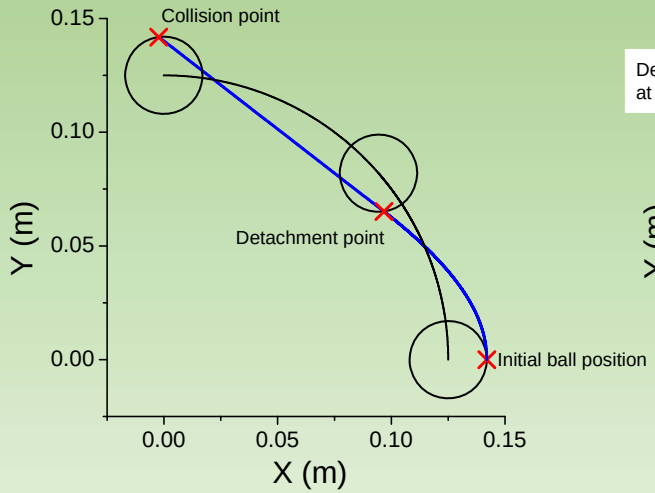

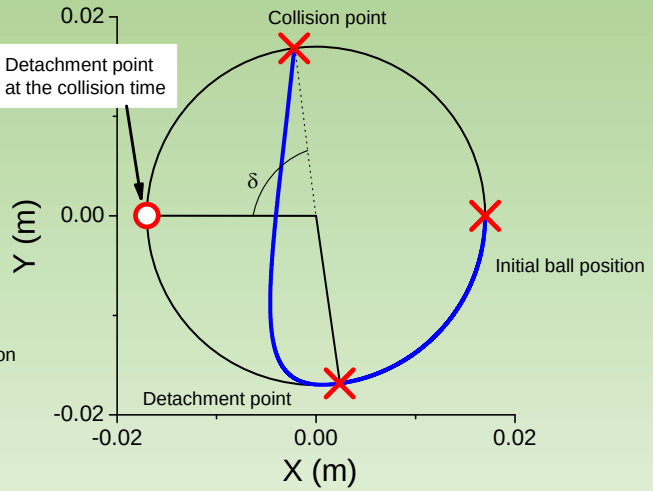

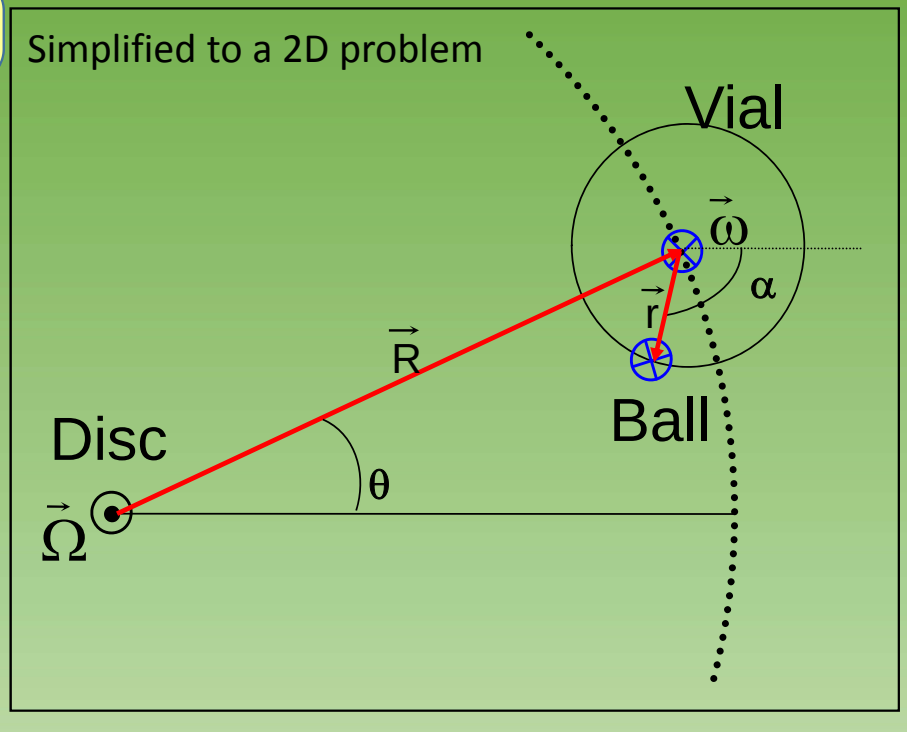

Strong approximations!

- Single ball approach
- The movement occurs in a plane.
- After collision, the ball moves stuck to the wall.
- No sliding is allowed.

Ipus et al. Intermetallics 16(2008)470

The ball detaches from the vial wall when the normal force becomes zero

$$N/m = \omega^2 r + \Omega^2 R\cos(\theta+\alpha) \Rightarrow t_d = \frac{1}{\omega+\Omega}\left[\arccos\left(\frac{-\omega^2 r}{\Omega^2 R}\right) - (\alpha_0+\theta_0)\right]$$

Detachment time, $t_d \propto 1/\Omega$

Flying time, $t_f \propto 1/\Omega$

$dN/dt = 1/(t_d+t_f) \propto \Omega$
Number of events in a period time independent of frequency

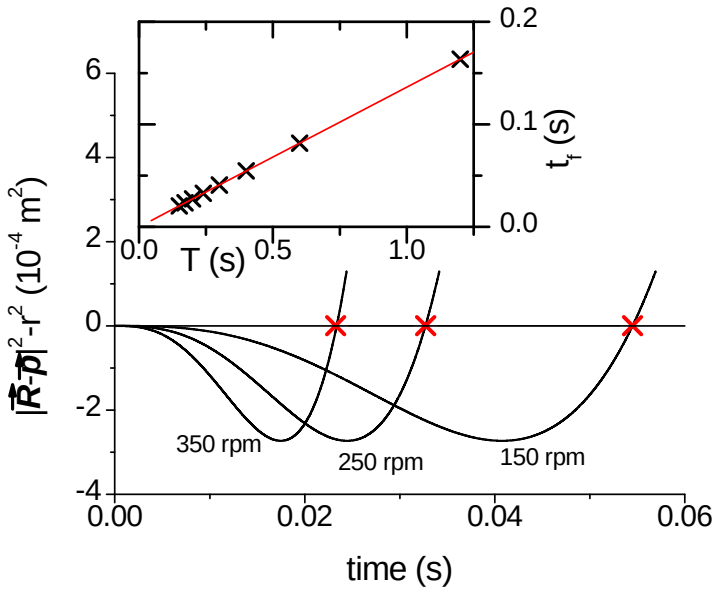

Ipus et al. Intermetallics 16(2008)470

Power released during milling

$$as \quad E_{colission} = C\Omega^2$$

$$P = \frac{dE}{dt} = \frac{dN}{dt} E_{colission} = C'\Omega^3$$

$$t_{eq} = t(\Omega / \Omega_0)^3$$

Equivalent milling time can be defined for experiments done at Ω referred to Ω_0

Ω dependence of vial temperature

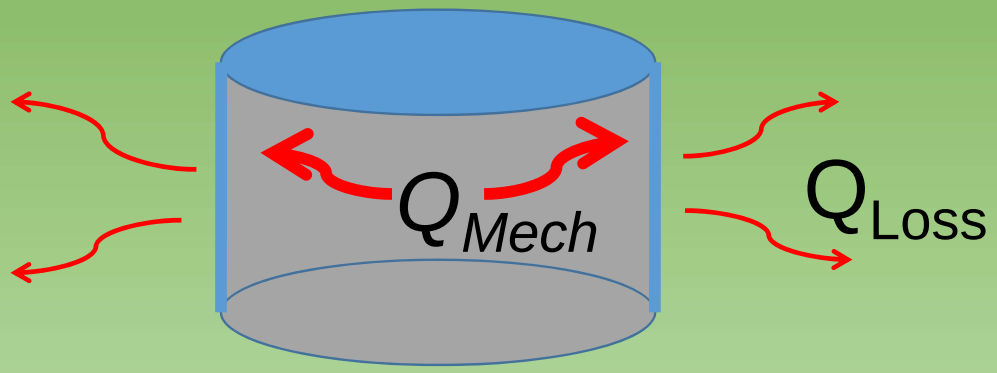

$$Q_{Mech} = A\Omega^3 t$$

$$\left|\frac{dQ_{Loss}}{dt}\right| = B\left|T_{IN} - T_{OUT}\right| = B\Delta T$$

$$\frac{dQ_{Total}}{dt} = A\Omega^3 - B\Delta T = C\frac{dT}{dt}$$

Stationary condition:

$$C\frac{dT}{dt} = A\Omega^3 - B\Delta T = 0$$

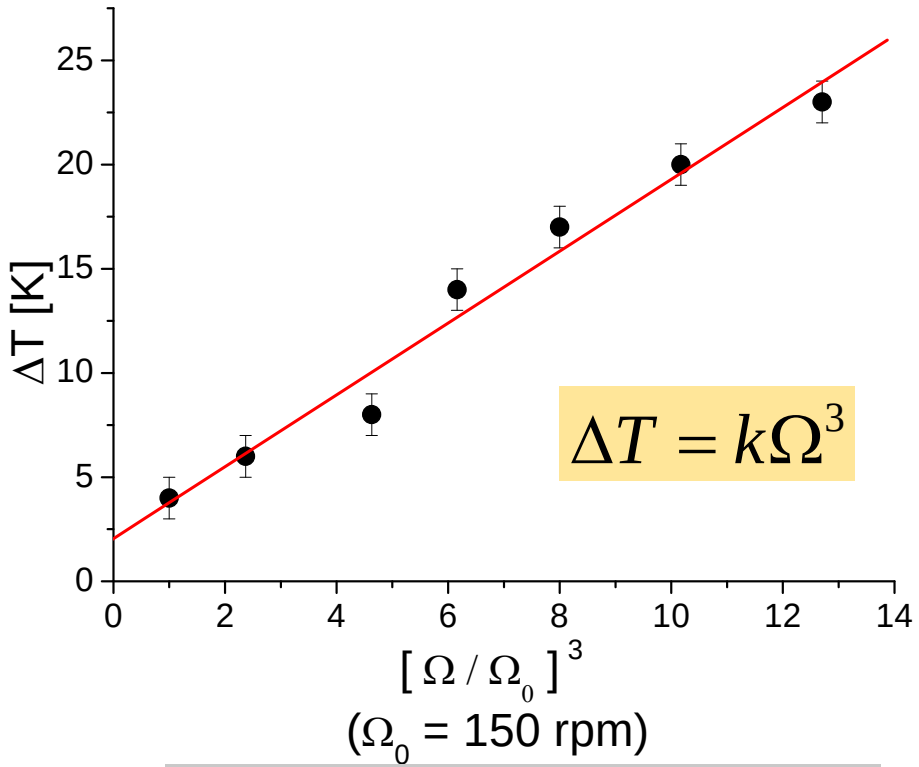

Blázquez et al. J. All. Compd.536S1(2012)9

In situ measurement of ΔT: GTMII

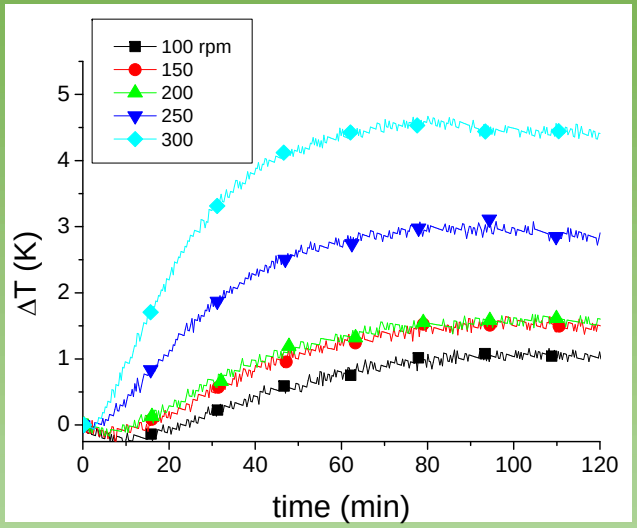

Integrating the equation:

$$I(t) = \int_0^t \Delta T dt = \frac{A}{B}\Omega^3 t - \frac{C}{B}\left(T(t) - T(0)\right)$$

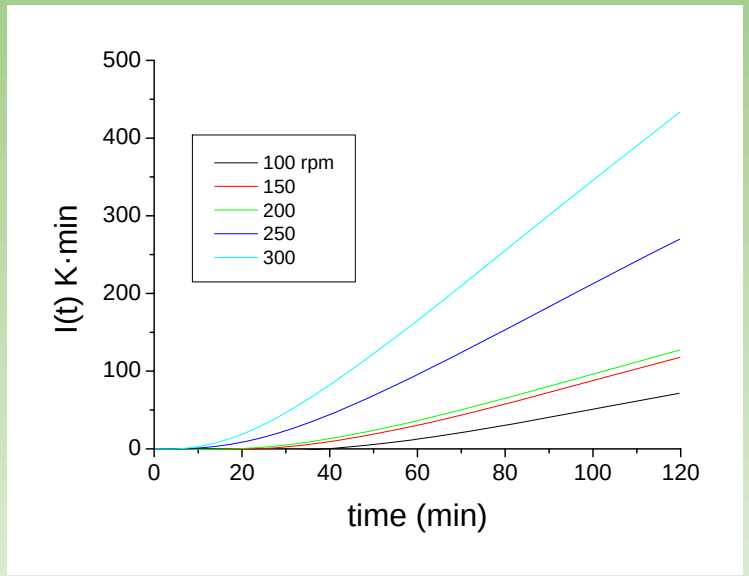

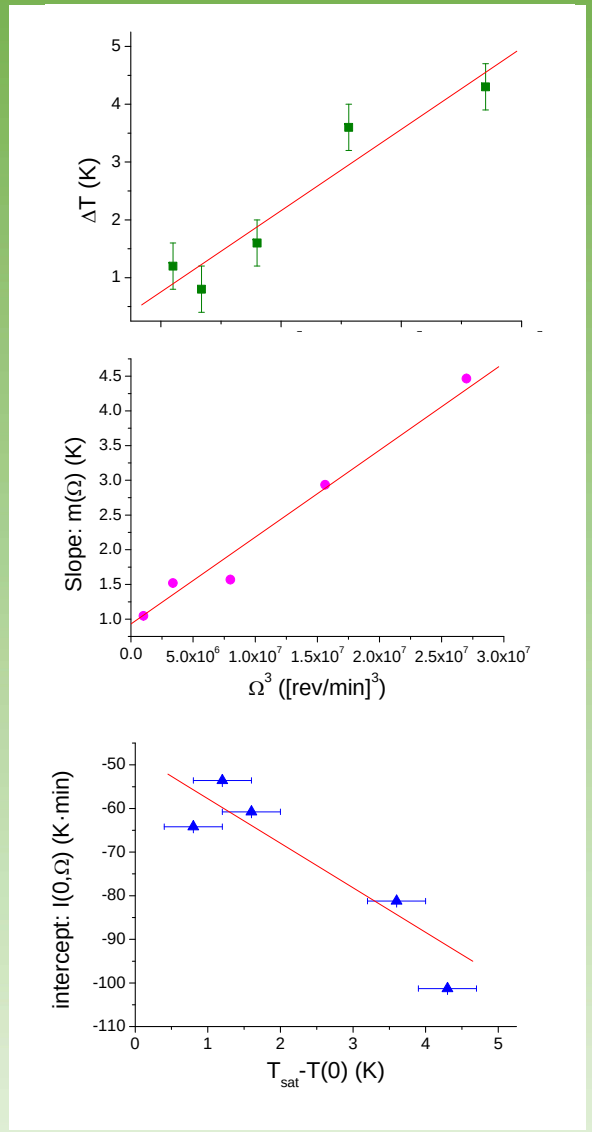

Microstructure of ball milled powders

X-ray diffraction: global microstructure

- Evolution of parameters following Ω^3 law

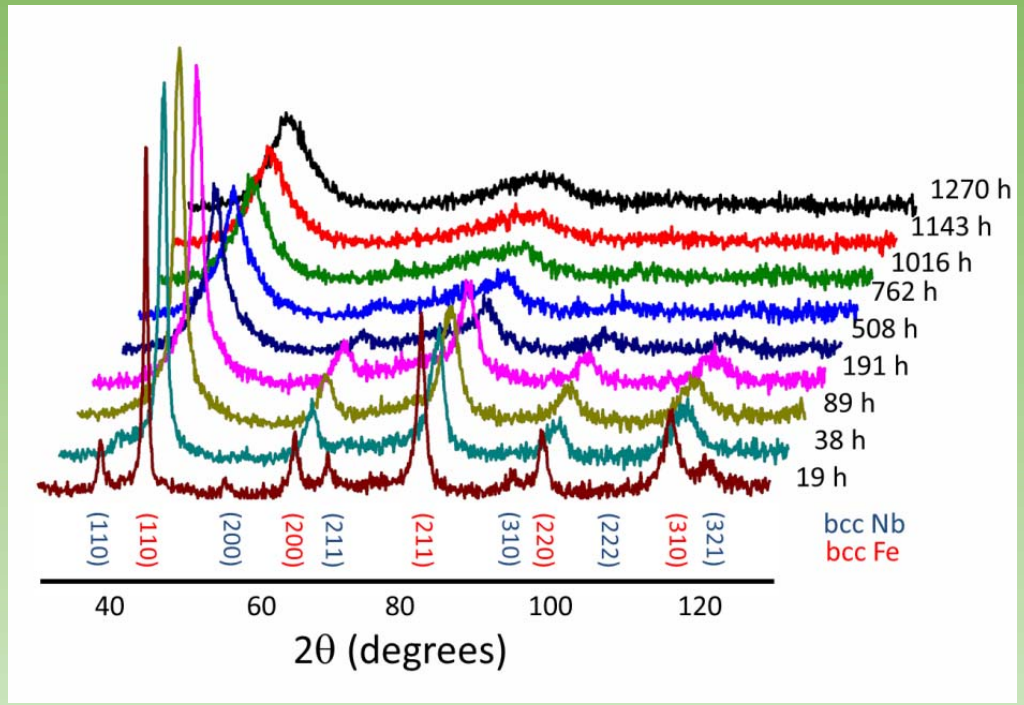

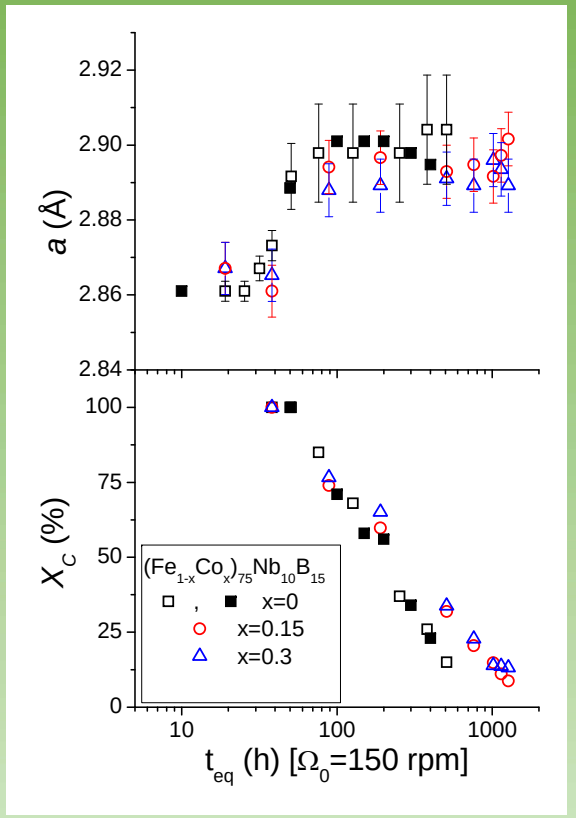

XRD patterns, lattice parameter and fraction of the bcc phase for $(Fe_{1-x}Co_x)_{75}Nb_{10}B_{15}$ as a function of equivalent milling time

Ipus et al. J.All.Compd.496(2010)7

^{57}Fe Mössbauer spectroscopy: local neighborhood of Fe

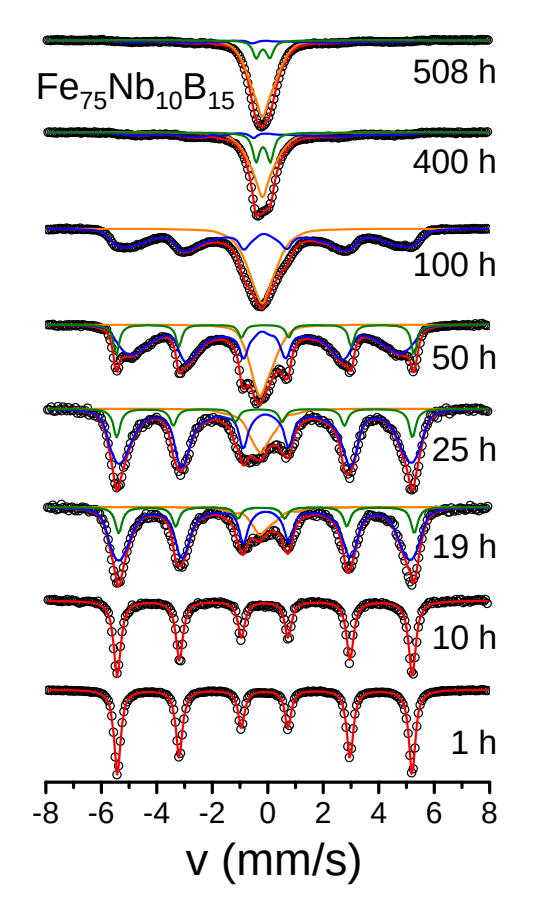

- ✓High sensibility to paramagnetic amorphous
- ✓Good correlation with magnetic measurements

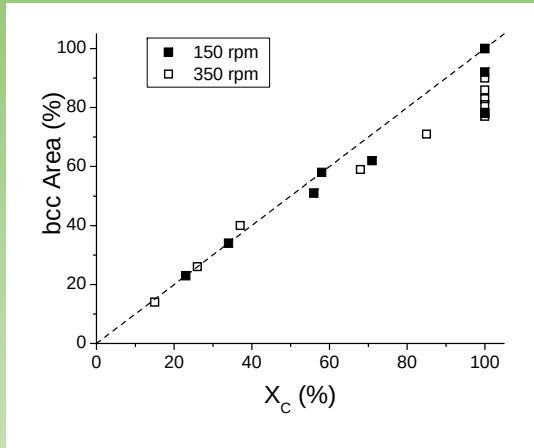

Correlation between Mössbauer and XRD crystalline fractions

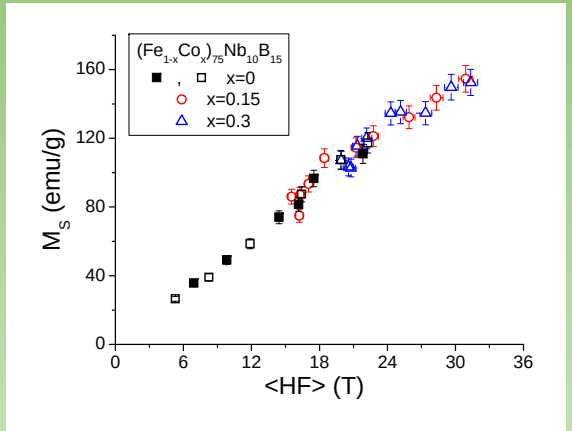

Correlation between hyperfine field and saturation magnetization

Ipus et al. Intermetallics 16(2008)1073

Ipus et al. J.All.Compd.496(2010)7

Estimation of compositions of nanocrystals from Mössbauer in supersaturated solid solutions

Blázquez et al. J.All.Compd.610(2014)92

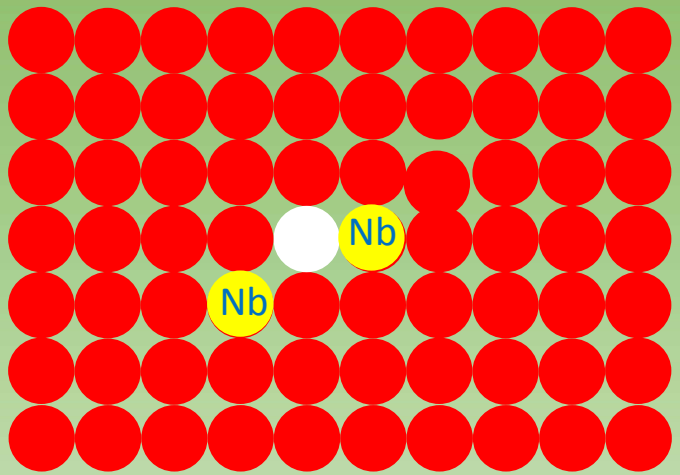

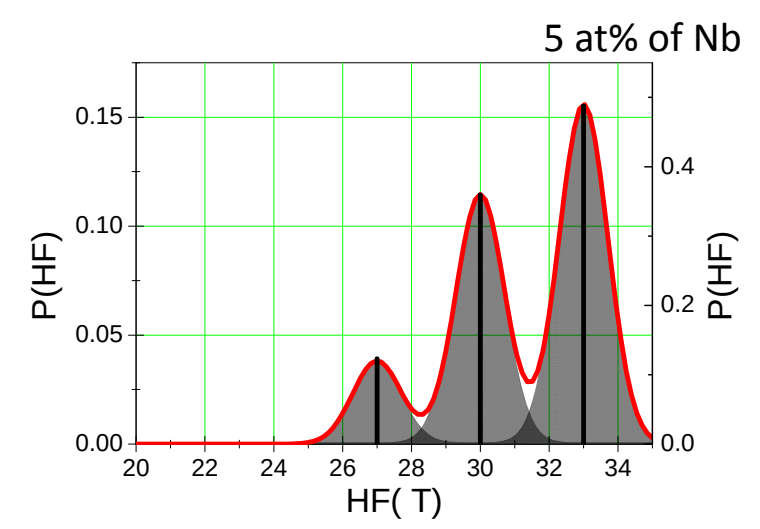

Probability of n Nb atoms as NN or NNN

$$P(n) = \frac{14!}{(14-n)!n!} C(Fe)^{14-n} C(Nb)^{n}$$

- ✓A pure bcc Fe neighborhood has HF=33 T
- ✓Fe atoms in the vicinity of Nb impurities have a reduction of ΔHF ~-3 T per Nb atom as NN or NNN

Estimation of compositions of nanocrystals from Mössbauer in supersaturated solid solutions

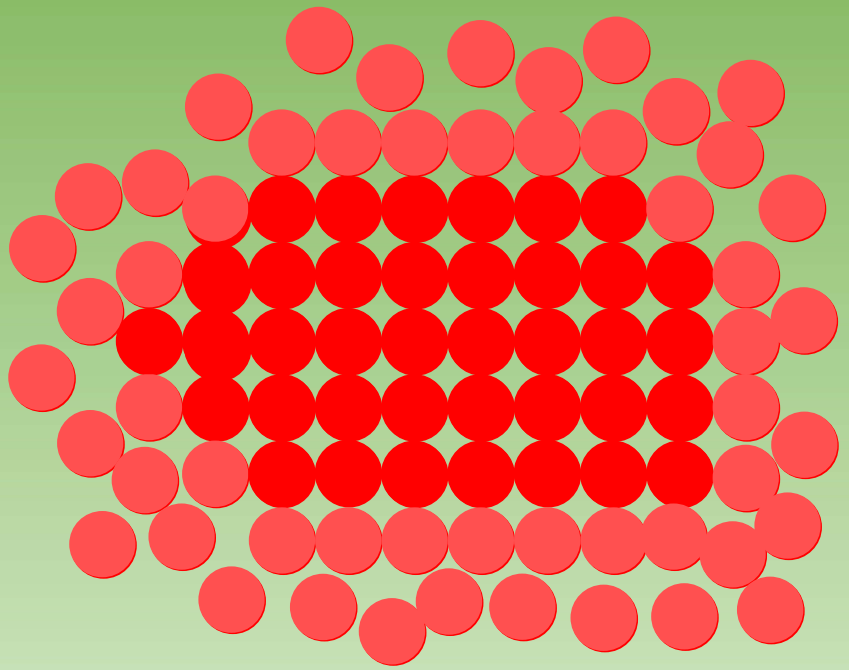

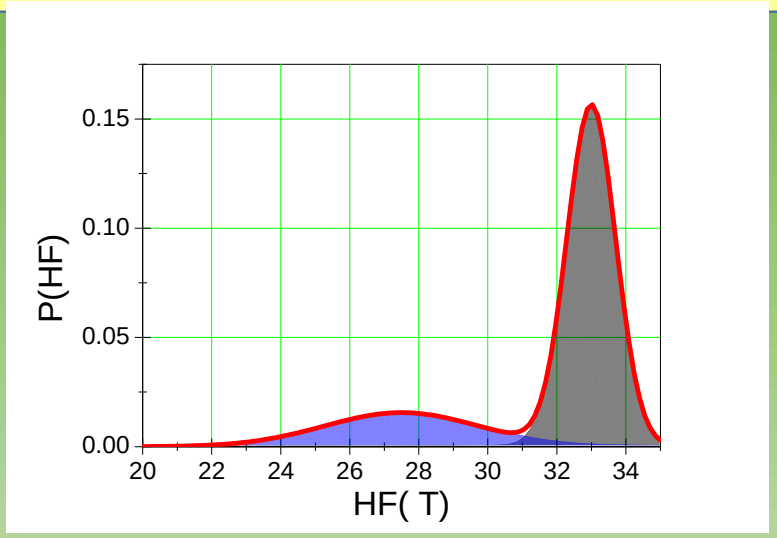

Probability of Fe atom at interface

$\sim 1/D$

✓Fe atoms at interface have a reduction in HF

Miglierini and Greneche J. Phys.: Cond. Matter 9 (1997) 2303

Estimation of compositions of nanocrystals from Mössbauer in supersaturated solid solutions

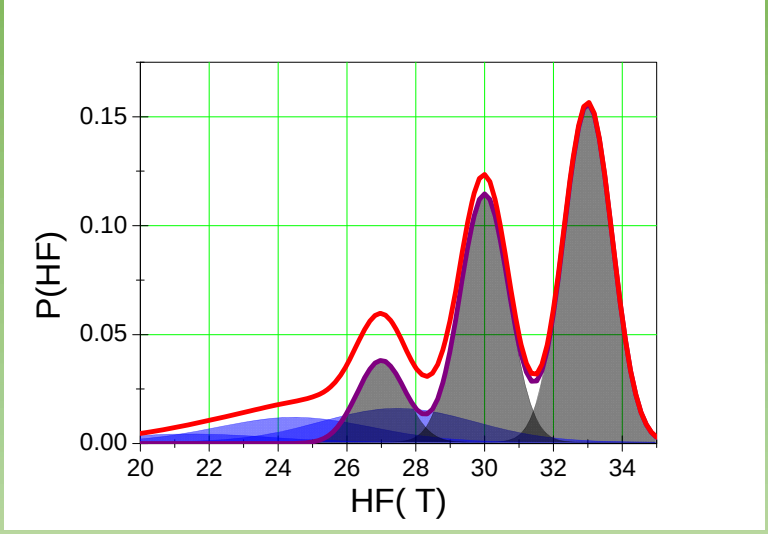

✓The highest HF contributions are less affected by interface

✓Composition can be extracted from the ratio of these contributions

$$\frac{P(1)}{P(0)} = \frac{14\left[1-C(Nb)\right]^{13} C(Nb)}{\left[1-C(Nb)\right]^{14}}$$

$$C(Nb)^{W} = \frac{14}{15} C(Nb) = \frac{14}{15} \frac{\frac{P(1)}{P(0)}}{\left[14+\frac{P(1)}{P(0)}\right]}$$

Estimation of compositions of nanocrystals from Mössbauer in supersaturated solid solutions

- Experimental application to mechanical alloying of $Fe_{94.4}Nb_{5.6}$

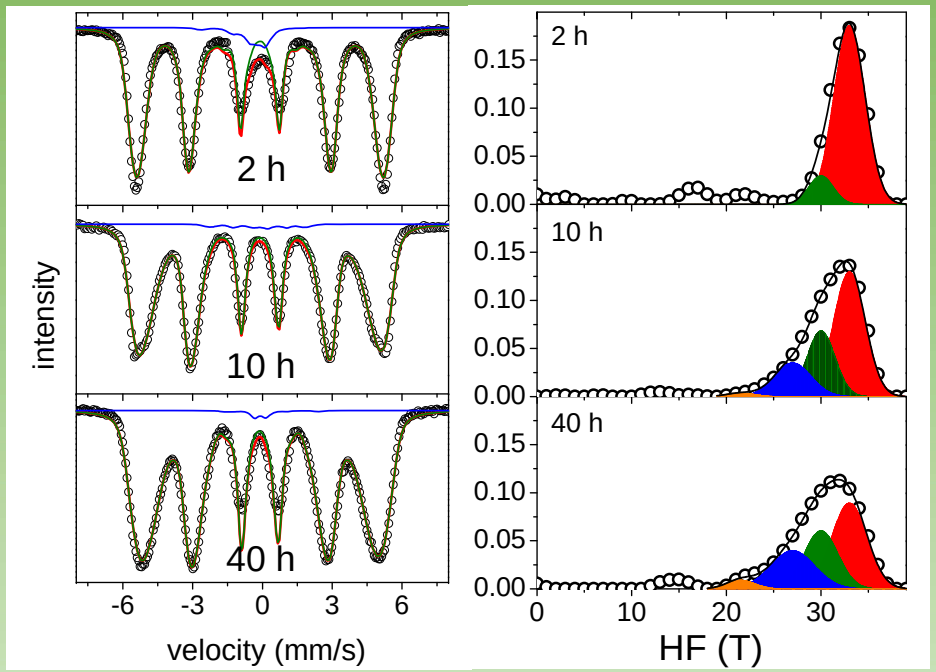

$$C(Nb)^{w} = \frac{14}{15}\frac{\frac{P(1)}{P(0)}}{\left[14+\frac{P(1)}{P(0)}\right]}$$

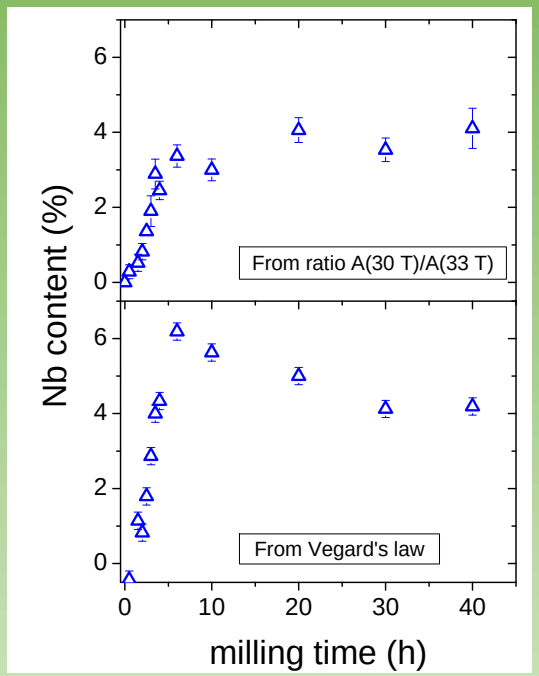

- ✓Spectra fitted using two hyperfine field distribution to determine the experimental HF distribution, HFD^{exp}
- ✓Fitting of high field range of HFD^{exp} using Gaussian functions at fixed HF (B-free) and at free HF (B-containing)

Electron microscopy techniques

Two length scales

✓Micrometric powder particles: SEM

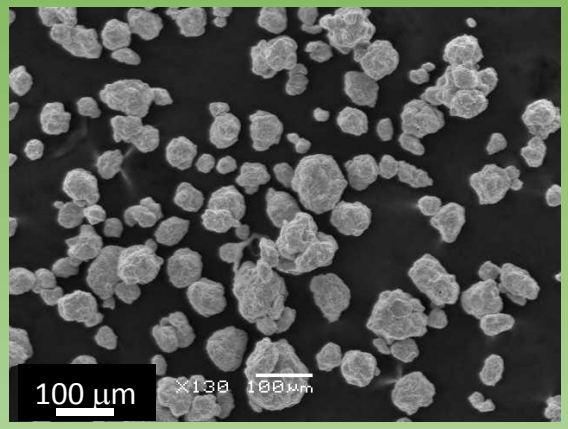

✓Nanocrystalline and amorphous phases: TEM

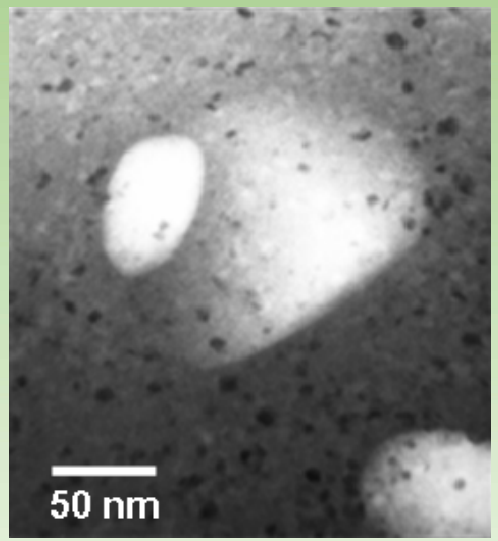

Sample preparation: Scanning Electron Microscopy

Dispersing powder on carbon film:

- ✓Particle size distribution, morphology (secondary electrons)
- ✓Detection of inclusions (back scattered electrons)
- ✓Microanalysis: compositional homogenization

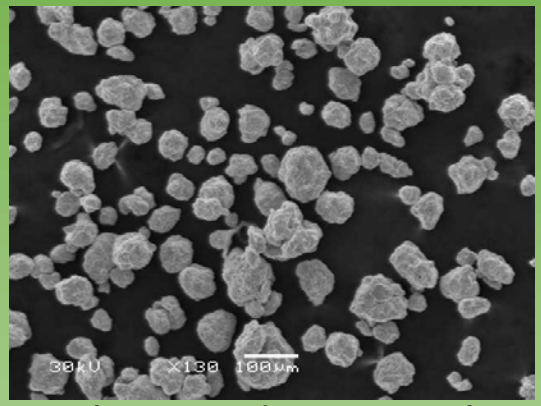

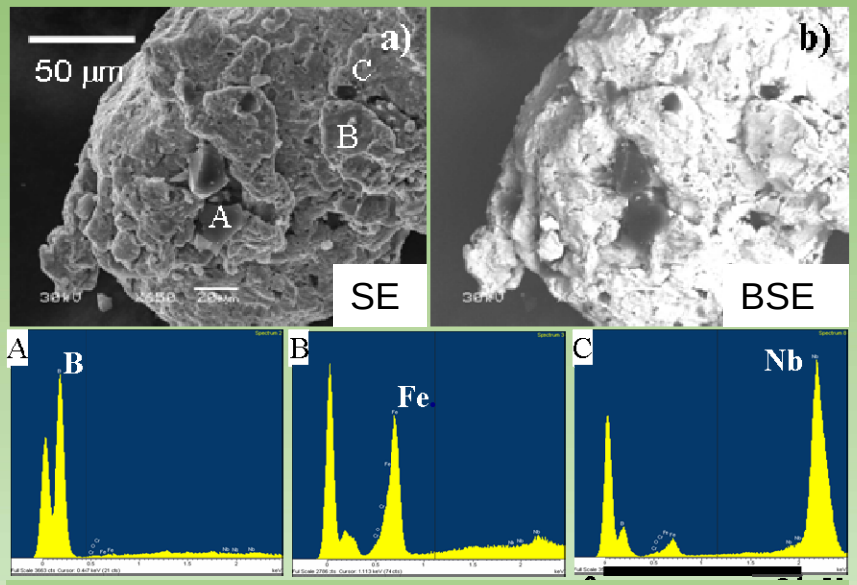

$Fe_{75}Nb_{10}B_{15}$: Initial stages of milling: powder particles formed by chips of the starting phases

Ipus et al. Intermetallics 16(2008)1073

Focus ion beam:

- ✓Polished surface of a single powder particle
- ✓Detailed view of inclusions

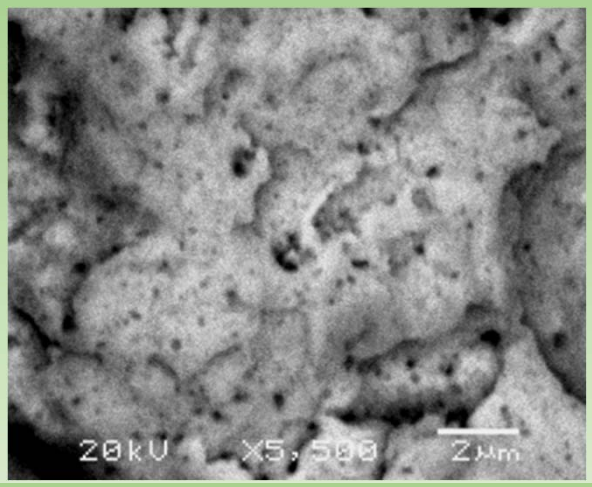

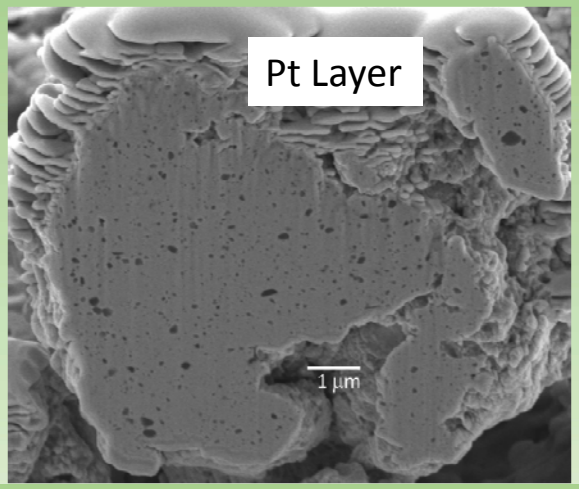

$Co_{62}Nb_6Zr_2B_{30}$: long milling. BSE in conventional SEM (left) and SE in FIB (rigth)

Moreno et al. J. All. Compd. 585(2014)485

Blázquez et al. Met. Mat. Trans. E 2(2015)131

Sample preparation: Transmission Electron Microscopy

- ✓Non-trivial sample preparation
- ✓Using lift-out method in FIB allows us to study a sample with constant thickness from a single powder particle
- ✓Detailed information on the nanostructure

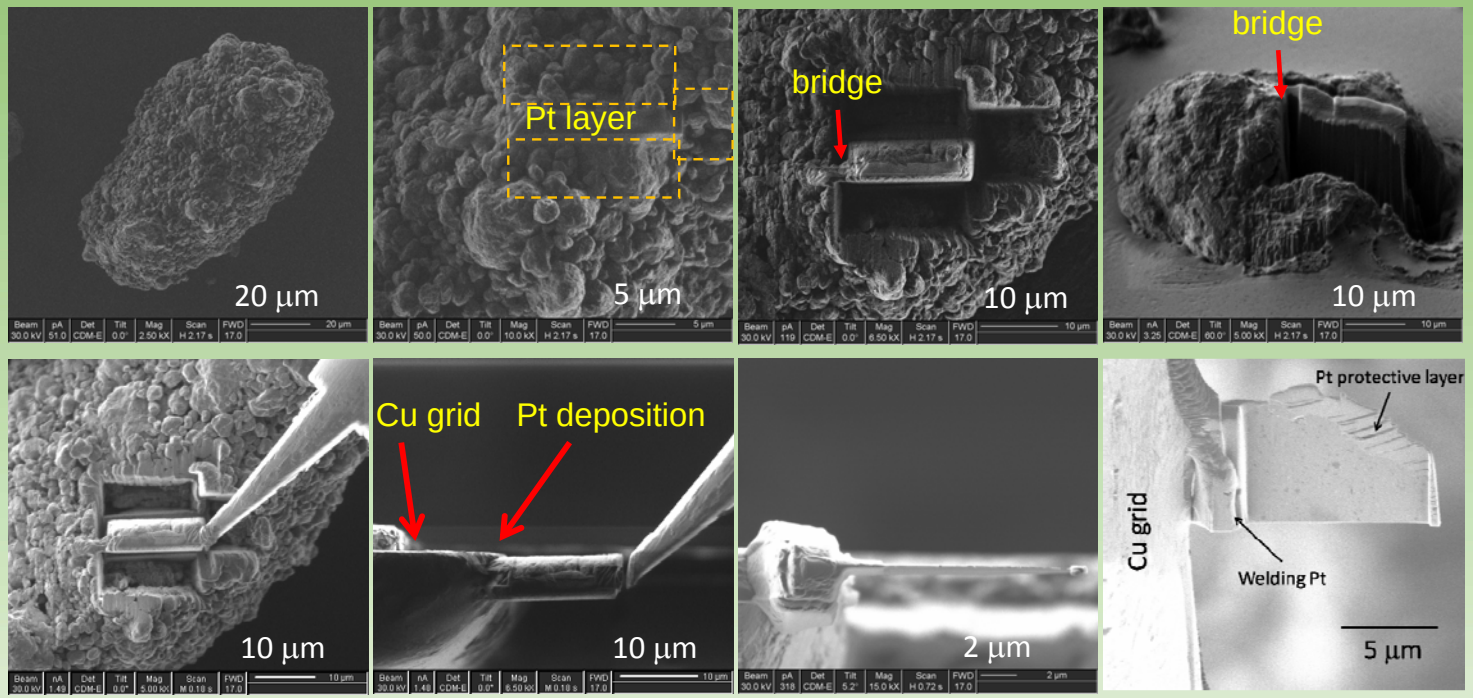

Lift-out method in Focus Ion Beam (FIB)

Ipus et al. Phil. Mag. 89(2009)1415

Powder particle size: SEM

- ✓Driven by fracture and cold welding
- ✓Following Ω^3 law
- ✓Temperature dependence can yield deviations from Ω^3 law for this parameter

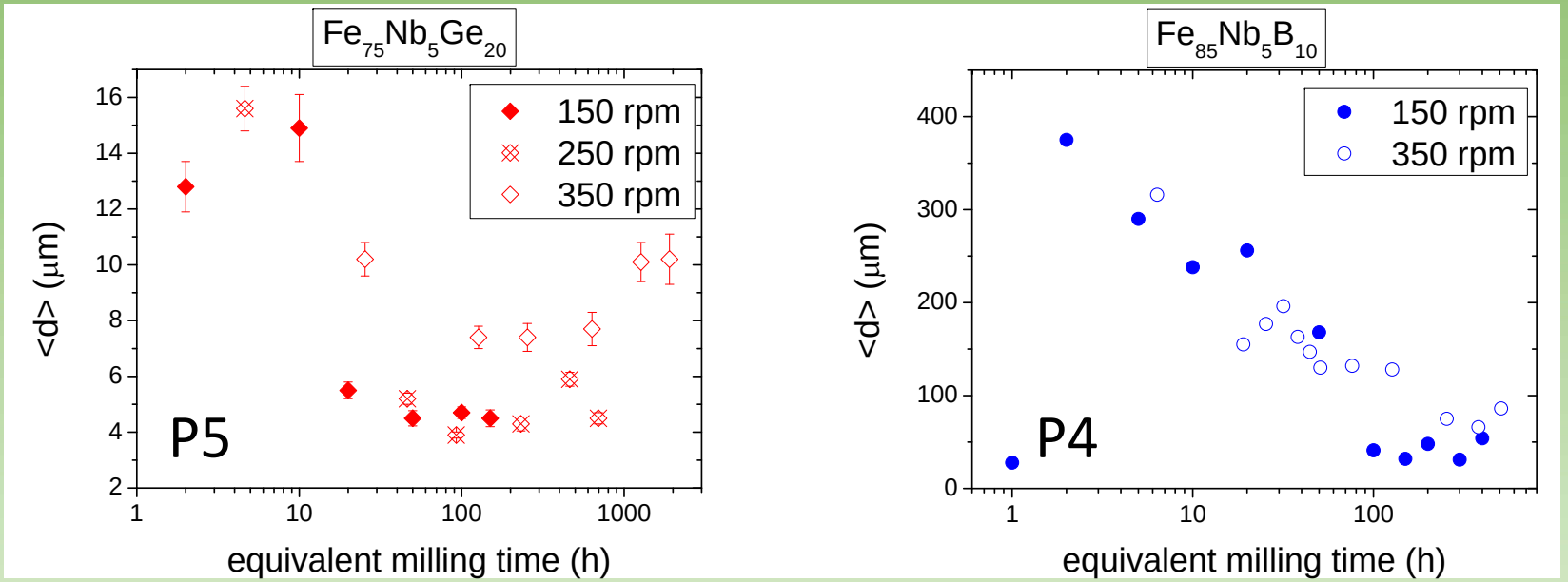

Powder particle size evolution as a function of the equivalent time for two compositions in two different mills

Blázquez et al. J. All.Compd.469(2009)169

Ipus et al. Intermetallics 16(2008)1073

Composition homogenization: SEM

- ✓Presence of a distribution
- ✓Saturation value could be affected by contamination

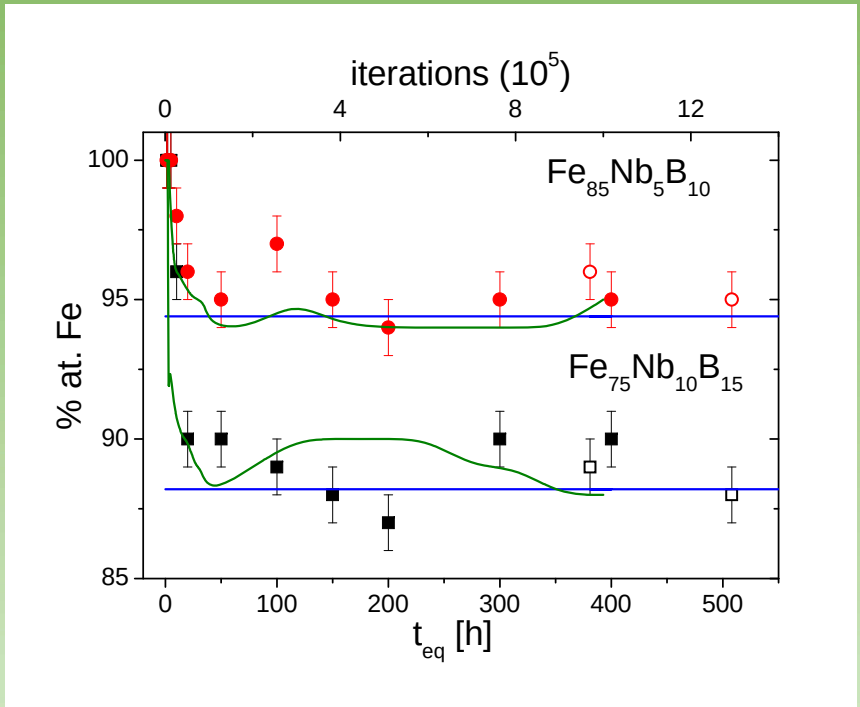

Average and distribution probability of the Fe content in a powder particle as a function of the equivalent time

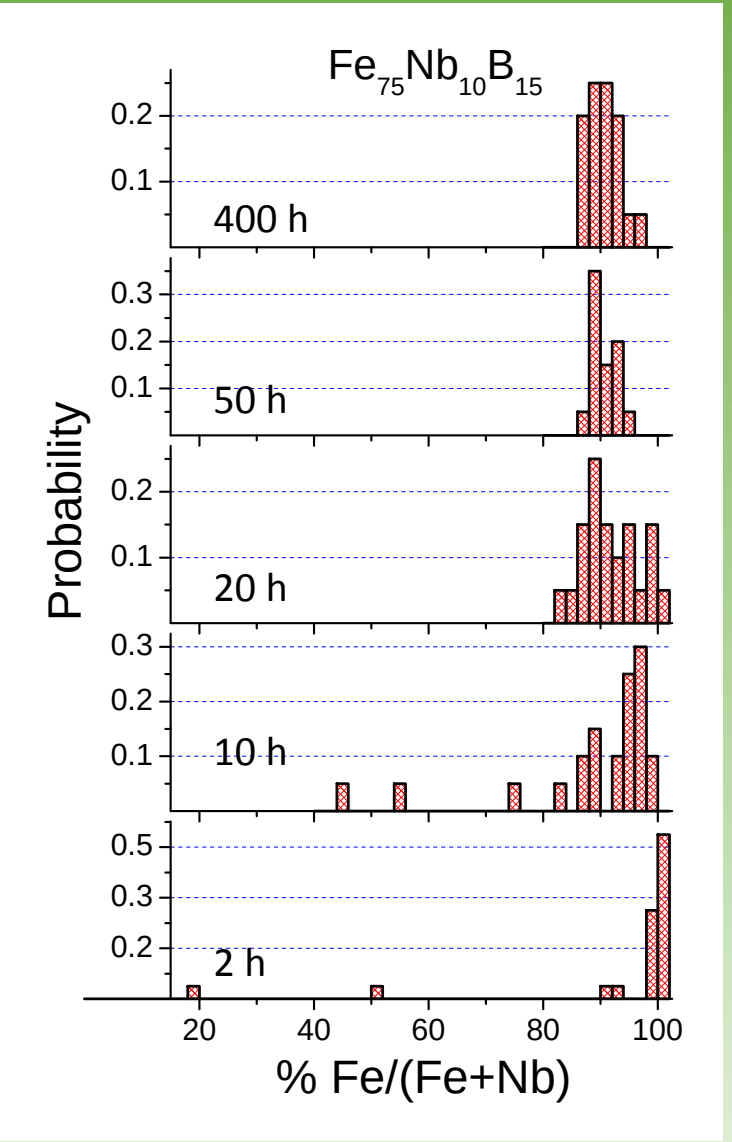

Ipus et al. Intermetallics 16(2008)1073

Contamination: SEM & TEM

- ✓Fe and Cr using steel milling media
- ✓Depends on powder composition
- ✓Following Ω^3 law

Blázquez et al. J. All.Compd.469(2009)169

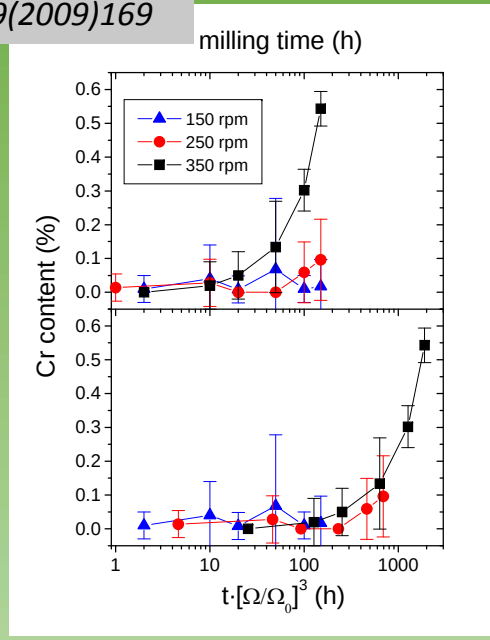

Cr content vs milling time for $Fe_{75}Nb_5Ge_{20}$ alloy using hardened steel balls

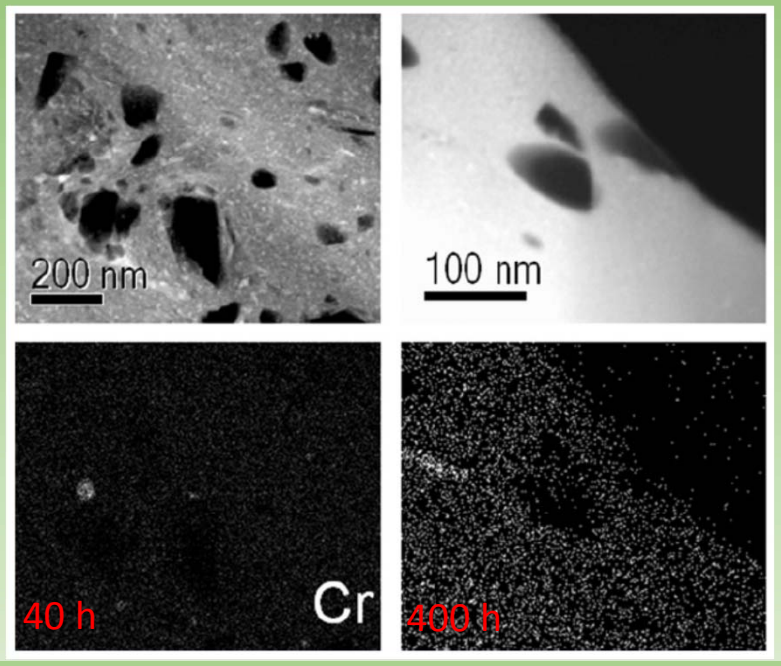

HAADF images and Cr EDX-maps for $Fe_{75}Nb_{10}B_{15}$ alloy

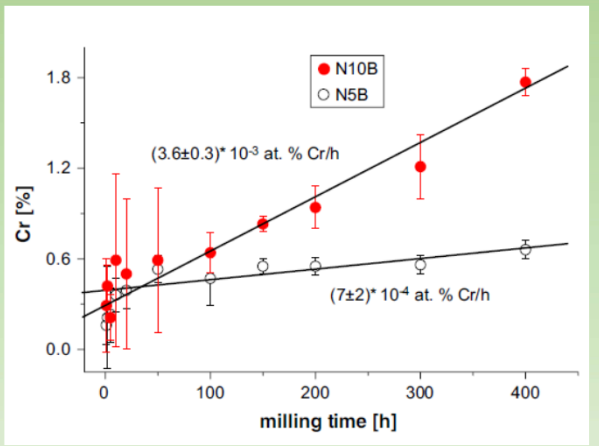

Cr content vs milling time for Fe-Nb-B alloys using hardened steel balls

Ipus et al. Intermetallics 16(2008)1073

How different elements incorporate to the alloy? Ductile materials: Fe and Nb

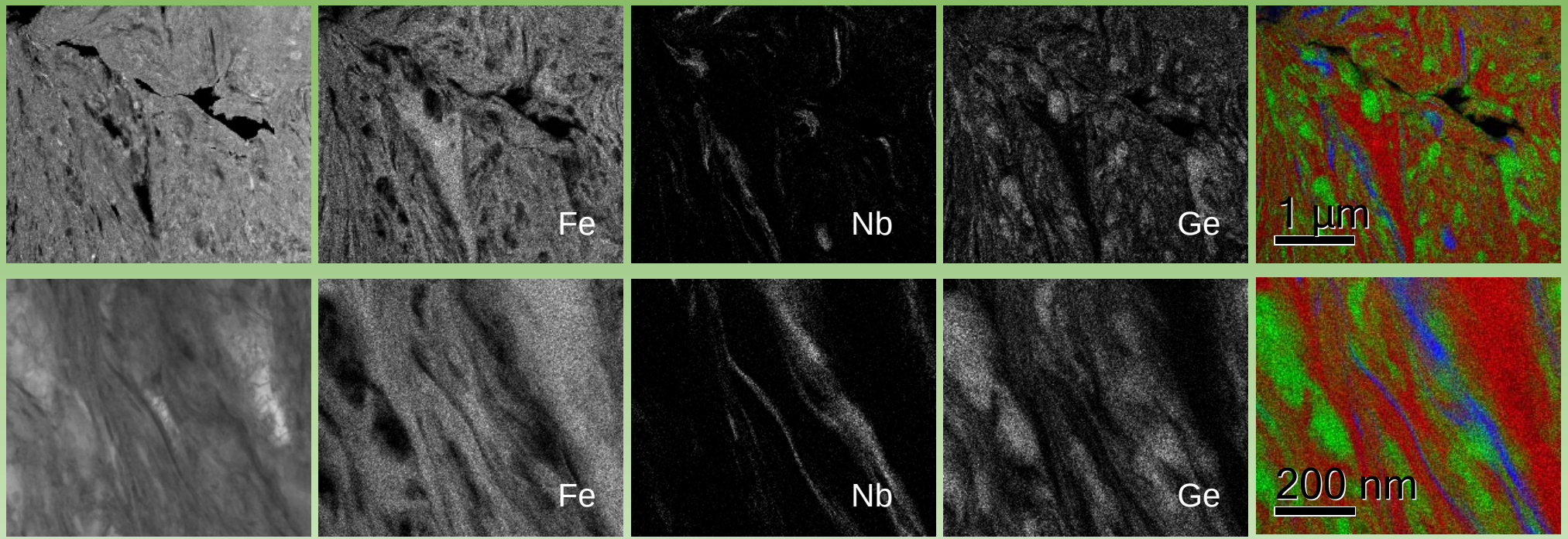

$Fe_{75}Nb_5Ge_{20}$: Supersaturated solid solution α-Fe(NbGe) nanocrystals after t_{eq}=46 h

Ipus et al. J.All.Compd.86(2009)505

How different elements incorporate to the alloy? Brittle materials: B and Ge

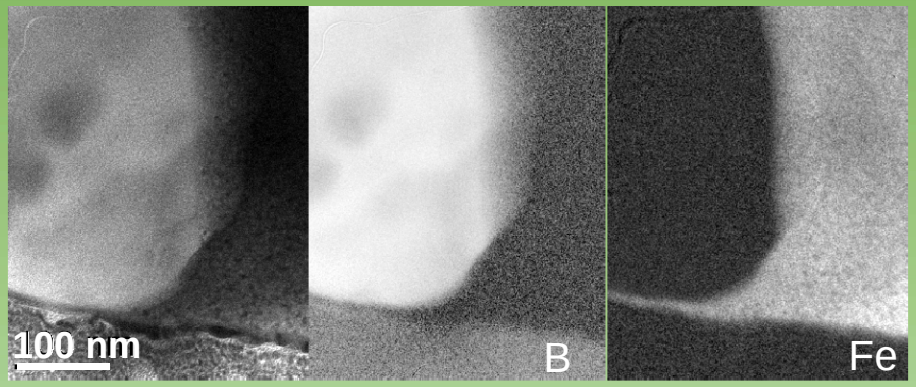

Ipus et al. Phil.Mag.89(2009)145

Fe-Nb-B: Inclusions highly enriched in boron after t_{eq}=508 h milling

Ipus et al. J.All.Compd.86(2009)505

Fe-Nb-Ge: Ge completely disolved in matrix after t_{eq}=508 h milling

Boron integration

- Present in both soft (e.g. Finemet) and hard (e.g. Nd-Fe-B) magnetic compositions

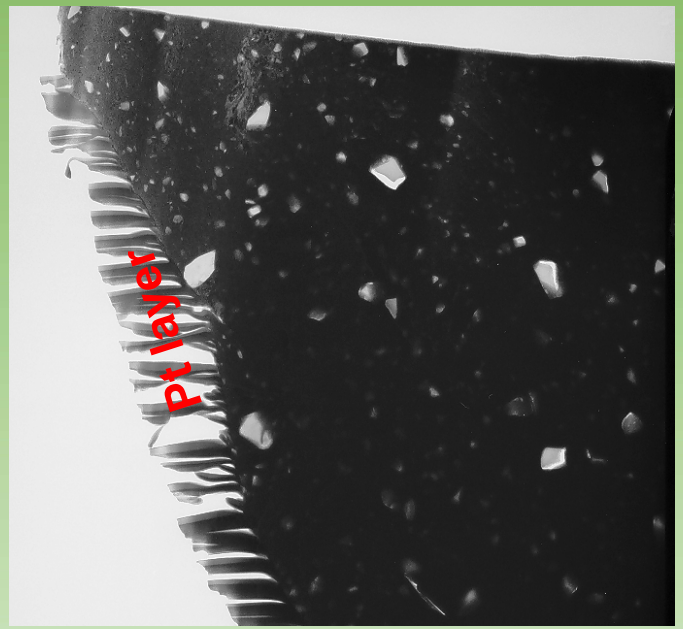

Bright field TEM image of a $Fe_{75}Nb_{10}B_{15}$ sample after 40 h milling

Ipus et al. Phil.Mag.89(2009)145

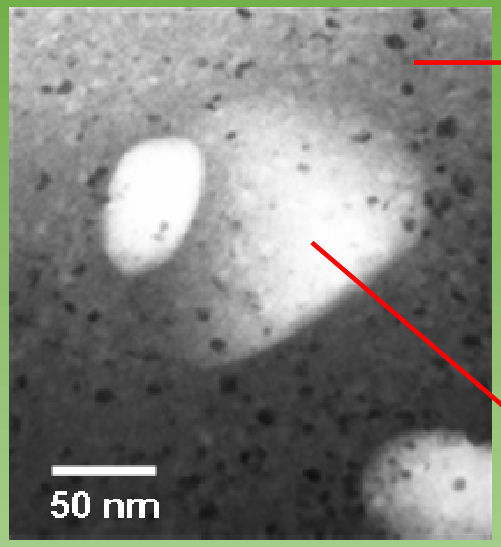

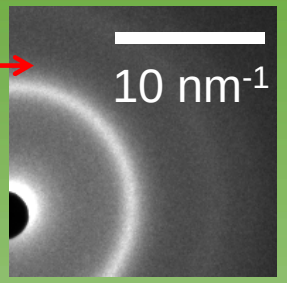

SAD on amorphous matrix + α-Fe nanocrystals

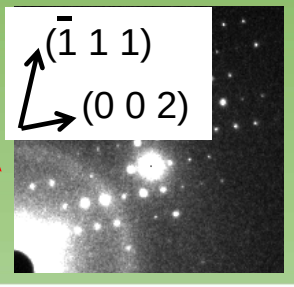

CBED on crystalline inclusion

BF image, SAED and CBED patterns of $Fe_{75}Nb_{10}B_{15}$ alloy milled 400 h

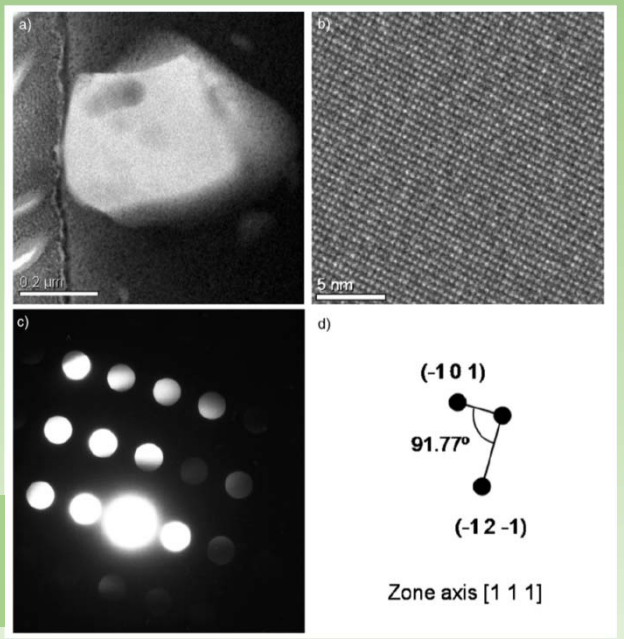

BF, HRTEM images and CBED pattern of a boron particle in $Fe_{85}Nb_5B_{10}$ alloy milled 400 h

- ✓Analytical results show presence of B in the matrix
- ✓Presence of almost pure boron inclusions
- ✓Actual matrix composition deviates from the nominal one

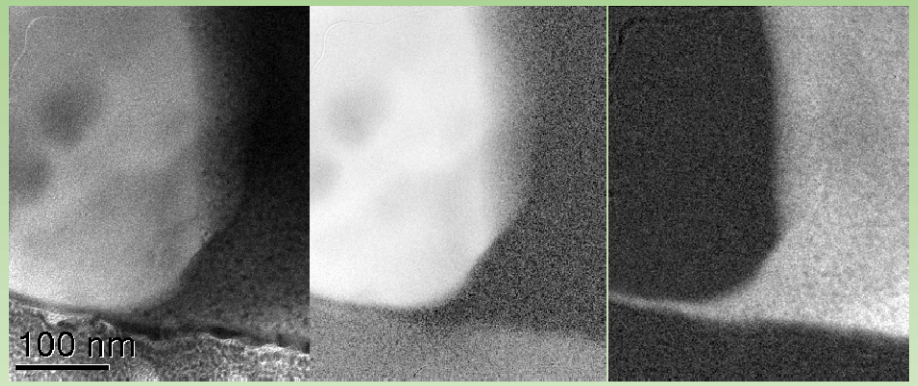

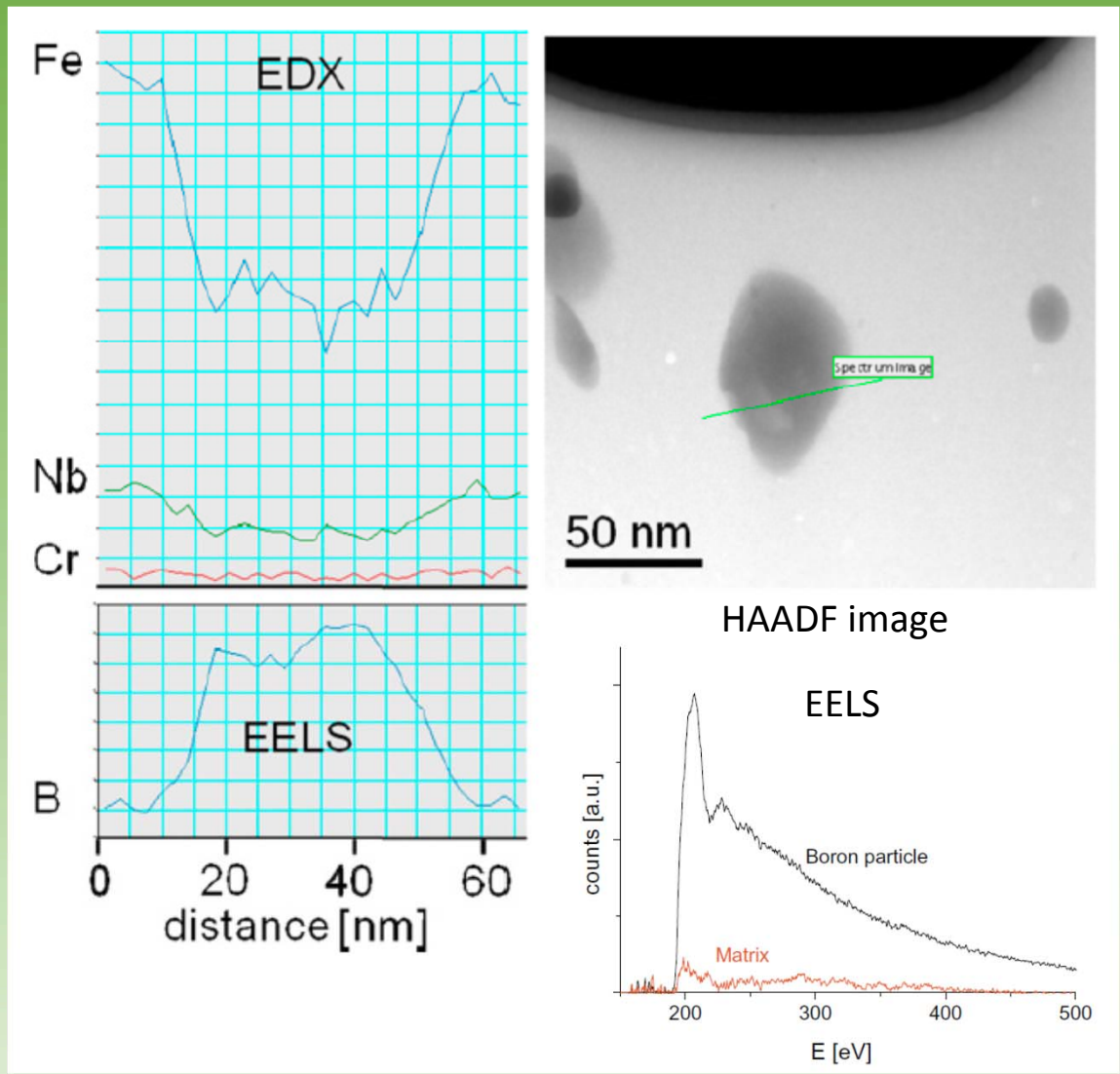

Ipus et al. J. All. Compd.553(2013)119

Effect of starting B microstructure

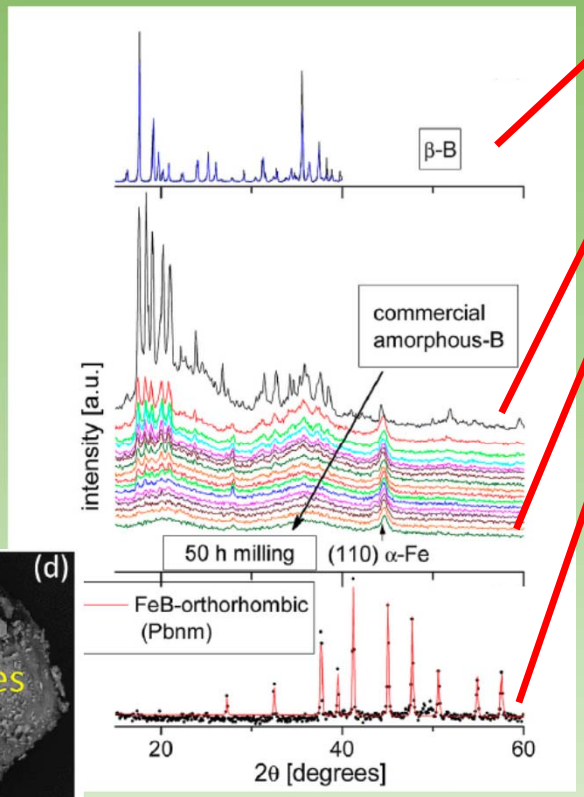

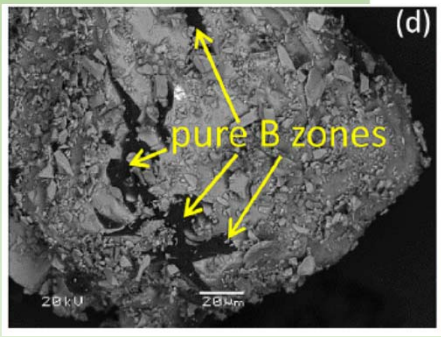

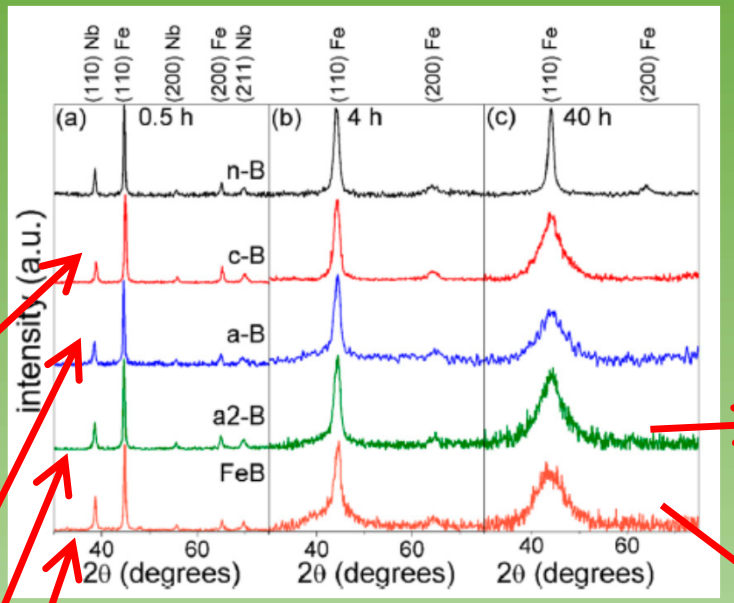

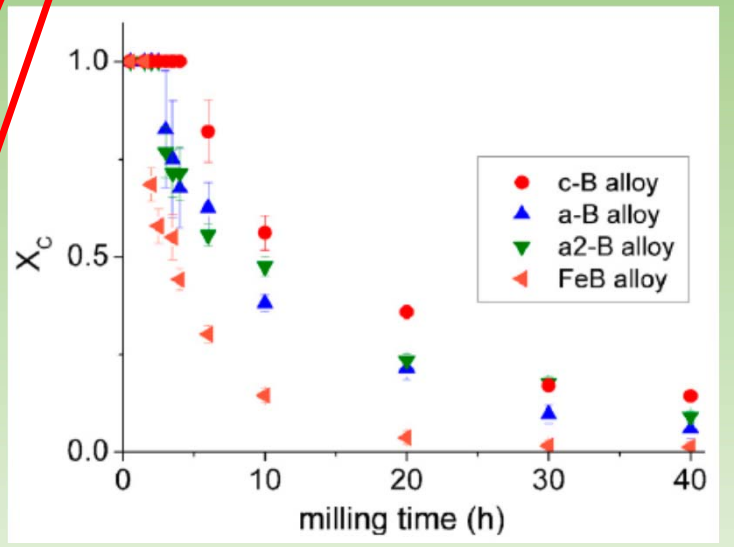

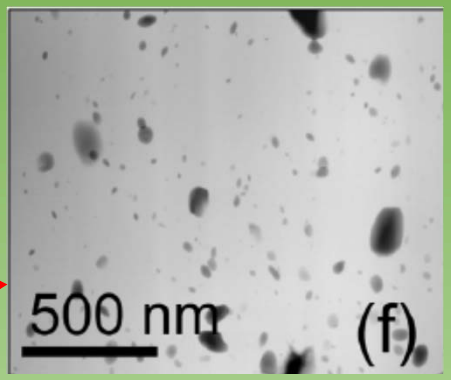

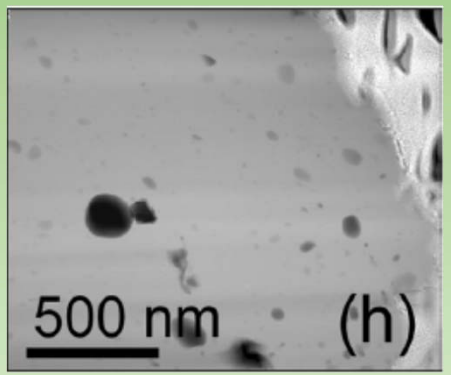

Ipus et al. Intermetallics 49(2014)98

- Comparison with melt-spun ribbons allows us to estimate the actual boron content in the matrix
- Curie temperature, very sensitive to B content in Fe-based alloys

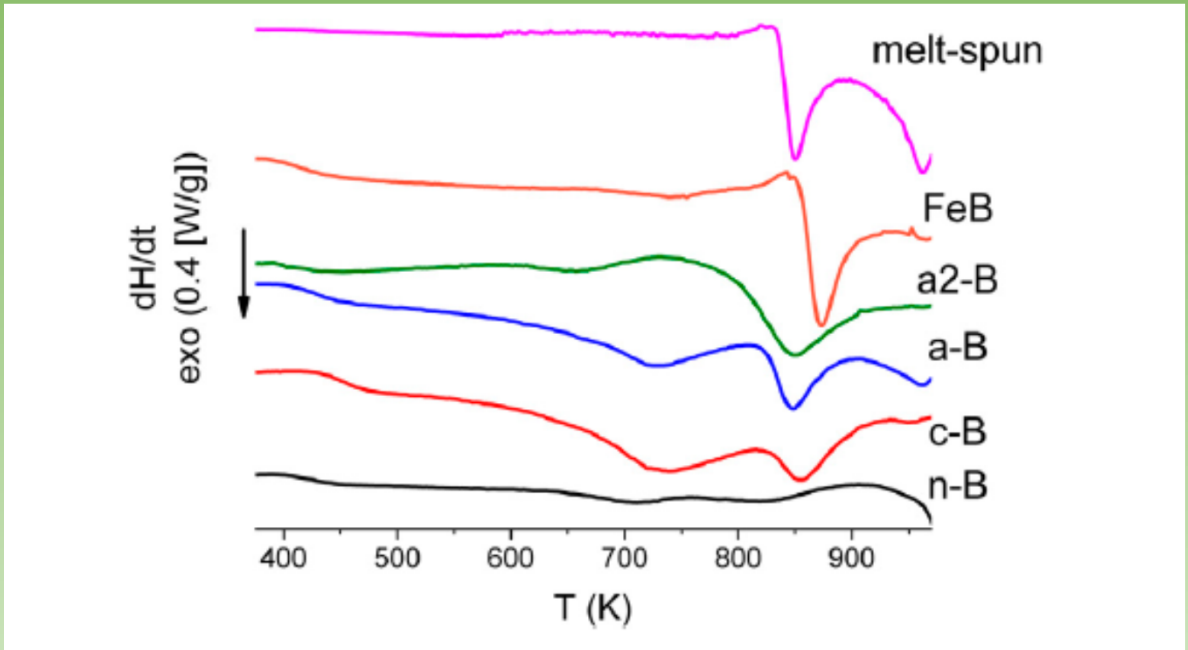

Differential scanning calorimetry on melt-spun ribbon and mechanically alloyed powders

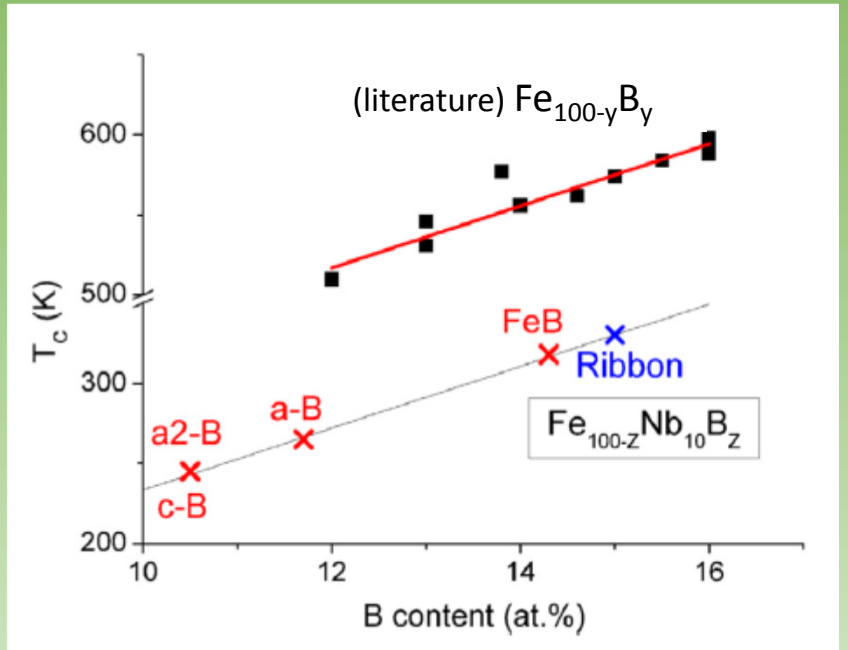

Estimation of the B content in the matrix after T_C values

Ipus et al. Intermetallics 49(2014)98

Magnetic properties of ball milled powder

Effect of packing on hysteresis loops

- When the powder is not glued the extra mechanism for alignment yields a decrease in coercivity

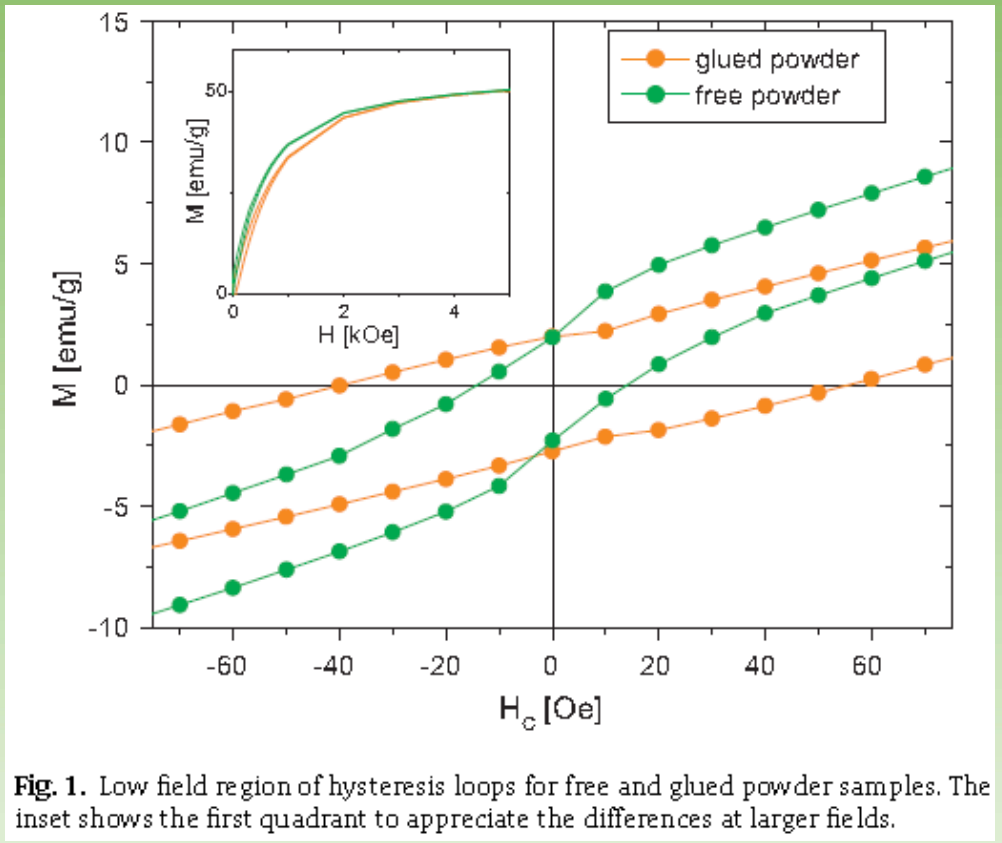

Fig. 1. Low field region of hysteresis loops for free and glued powder samples. The inset shows the first quadrant to appreciate the differences at larger fields.

Ipus et al. J.All.Compd.509(2011)1407

Spontaneous magnetization and coercivity

- Equivalent time approach is valid for a general interpretation

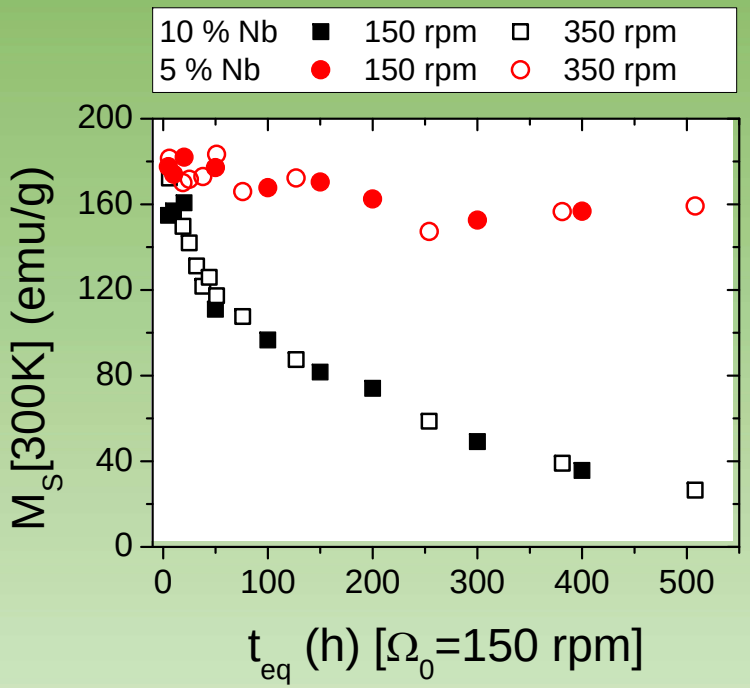

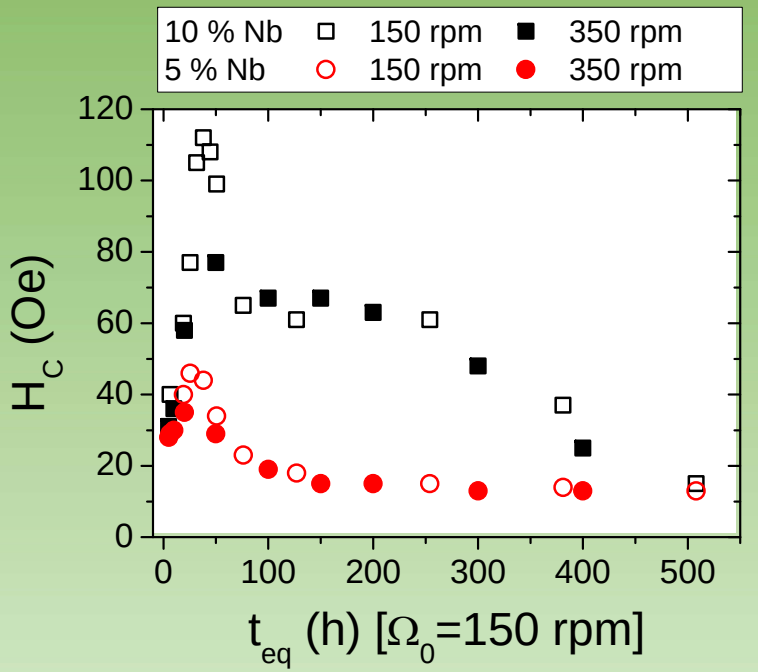

$Fe_{85-2x}Nb_{5+x}B_{10+x}$: mechanical amorphization (x=5) and supersaturated solid solution (x=0)

Ipus et al. J.All.Compd.509(2011)1407

Magnetic anisotropy $K_{eff} \sim H_C M_S$

- At short milling times increase due to microstrain increase

- At long milling times, three contributions:

Shen et al. Phys. Rev. B 72(2005)014431

$$K_{eff} = \sqrt{\left(\frac{3}{2}\lambda_S \sigma_{ma}\right)^2 + \left[\left(\frac{3}{2}\lambda_S \sigma_{mi}\right)^2 + X_C{}^2 K_1^2\right]\frac{D^3 K_{eff}^{3/2}}{A^{3/2}}}$$

- ✓ Long range magnetoelastic (powder size)
- ✓ Two average magnetic anisotropies
  - short range magnetoelastic (crystal size)
  - averaged magnetocrystalline characteristic of nanocrystalline materials

Hernando et al. Phys. Rev. B 51(1995) 3581

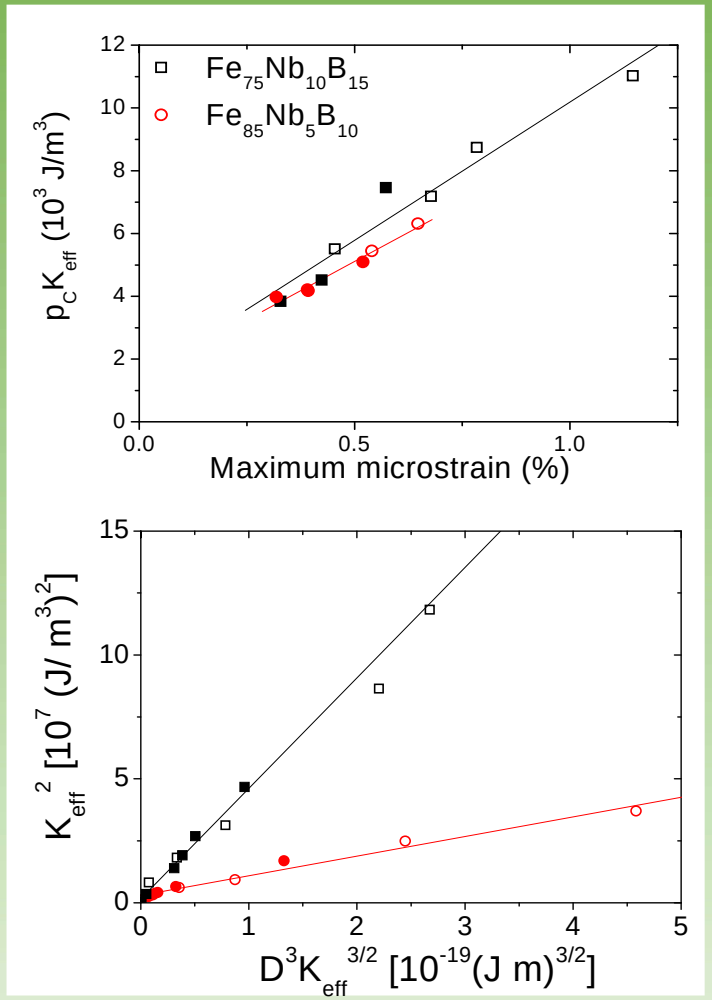

Ipus et al. J.All.Compd.509(2011)1407

Magnetocaloric effect on ball milled samples

Sevilla, December 11th 2015

Some examples on ball milling samples for MCE

Composition	Use of ball milling	Advantages	H (T)	$\|\Delta S_M\|$ (J kg^{-1}K^{-1})	T_{peak} (K)	Ref.
$Gd_5Si_{1.8}Ge_{1.8}Sn_{0.4}$	Crystal size reduction / amorphization	Hysteresis reduction	5	4.3	75	Sol. Stat. Comm. 147(2008)107
GdNiAl		New phase	5	8.9	36	Appl. Phys. A 80 (2005) 601
$Gd_5Si_2Ge_2$		Broadening	2	0.45	220	J.Mag.Mag.Mater. 320 (2008) 1479
Pr_2Fe_{17}			5	4.5	295	Acta Mater. 57 (2009) 1724
$Eu_8Ga_{16}Ge_{30}$		Low T enhancement	5	10	5	J. Appl. Phys. 117 (2015) 033903
$Ni_{2.18}Mn_{0.82}Ga_1$	One step (mechanical alloying)	Different melting points of the constituents	2	1.6	310	Sol. Stat. Comm. 148 (2008) 289
$Ni_{47}Mn_{40}Sn_{13}$			2	4.3/2.3	210/318	J. All. Compd. 598 (2014) 6
$Mn_{0.95}Cr_{0.05}As$	Intermediate step	Avoid volatilization of As	5	6.3/5.3	159/234	Phys. B 406 (2011) 2731
$Mn_{1-x}(Si,Al)_xAs$	Mechanical alloying		2	6.5	264	J. All. Compd. 479 (2009) 189
$MnAs_{0.97}P_{0.03}$		Hysteresis reduction	5	5.6/4.4	208/253	Appl. Phys. Lett. 100 (2012) 112407
$(Fe_{85}Co_{15})_{75}Nb_{10}B_{15}$		Amorphization	1.5	0.85	450	J. All. Compd. 496 (2010) 7
$Co_{62}Nb_6Zr_2B_{30}$			1.5	0.35	550	J. Appl. Phys. 115 (2014) 17A302
$(Fe_{70}Ni_{30})_{89}Zr_7B_4$		Metastable phases	0.5	0.18	342	IEEE Trans. Mag. 47 (2011) 2494
$Fe_{70}Ni_{30}$			1.5	0.65	363	J. Appl. Phys. 113 (2013) 17A918
$(Fe_{70}Ni_{30})Mo_4$			5	1.67	300	J. Elect. Mater. 43 (2014) 137
$Fe_{70}Zr_{30}$			1.5	0.43	225	Intermetallics 26 (2012) 52
$Fe_2MnSi_{1-x}Ge_x$	Precursor step (homogenization of composition)		5	1.6	270	Phys. B 328 (2003) 295
$La_{1-y}RE_yFe_{11.4}Si_{1.6}$		Reduction of annealing time	5	18	200	J. Appl. Phys. 102 (2007) 093906
$LaFe_{13-x}Si_x$			2	24	200	Intermetallics 18 (2010) 2301
$LaFe_{11.57}Si_{1.43}H_\delta$	Final step	Reactive milling	2	18	346	J. Appl. Phys. 102 (2007) 053906

Blázquez et al. Met. Mat. Trans. E 2(2015)131

Non-negligible demagnetizing field

Theoretical simulations using Arrot-Noakes EOS

- ✓Effect on magnetic entropy change ΔS_M
- ✓Strong effect on the field dependence of ΔS_M defined as $\Delta S_M = aH^n$
- ✓Strong effect on the field dependence of $RC = FWHM \cdot \Delta S_M$ defined as $RC = bH^m$

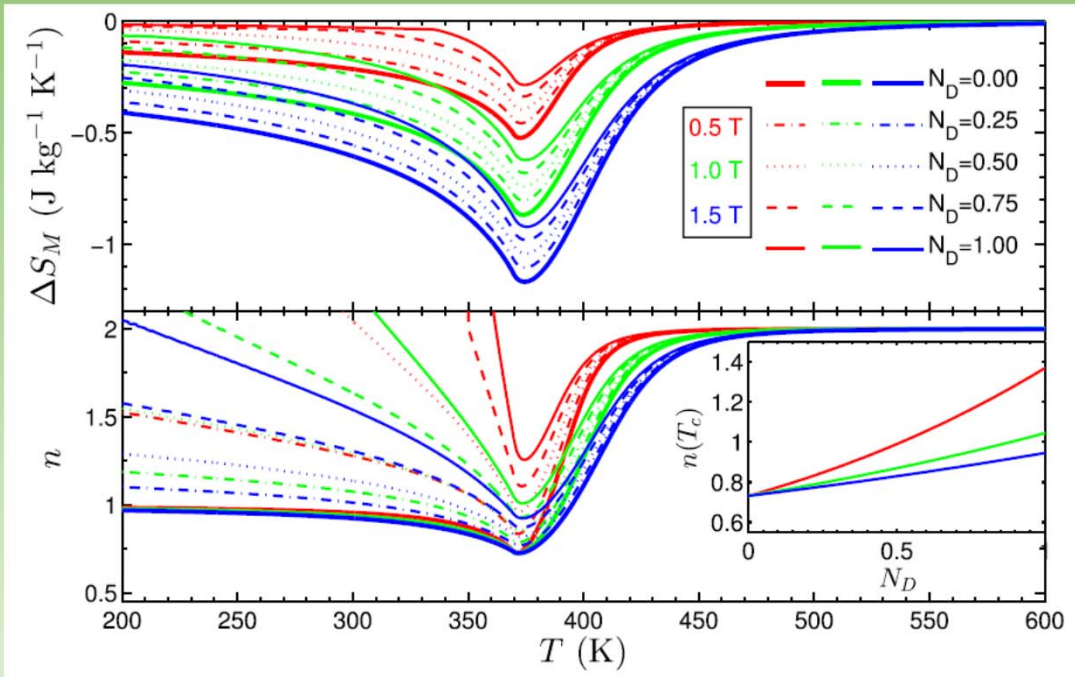

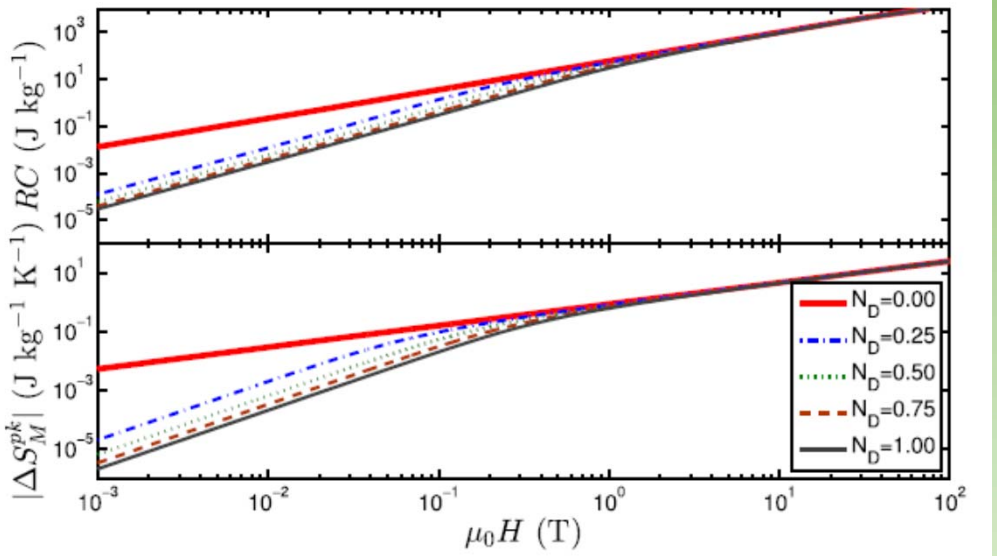

Demagnetizing field effect on magnetic entropy change, exponent n and refrigerant capacity Arrot-Noakes systems

Romero-Muñiz et al. Appl. Phys. Lett.104(2014)252405

Non-negligible demagnetizing field

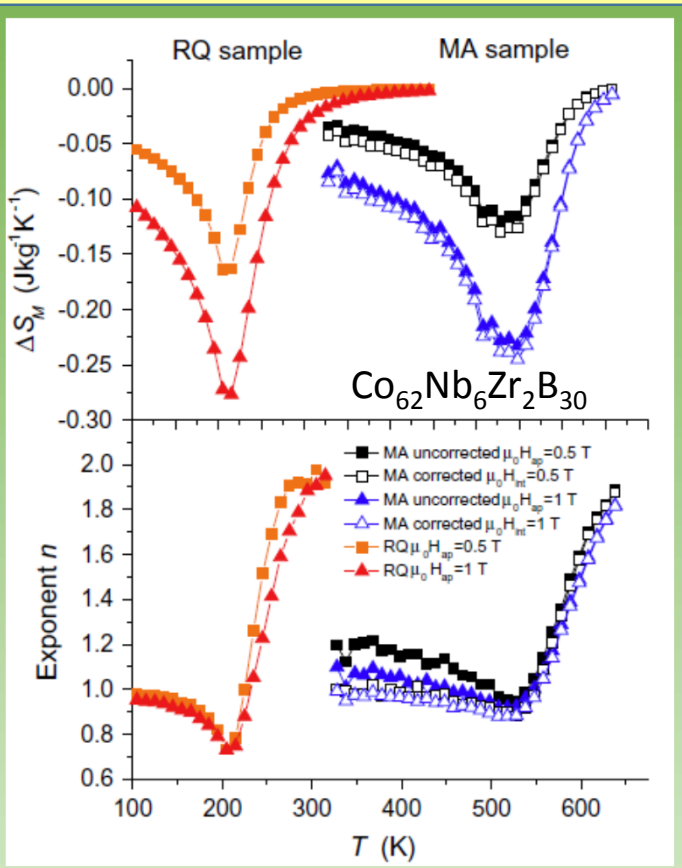

- ✓Experimental data: comparison between melt-spun ribbon (N_D~0) and milled samples (N_D~1/3)
- ✓Data corrected using $H=H_{appl}-N_DM$
- ✓Theoretical predictions of field dependence of MCE is recovered

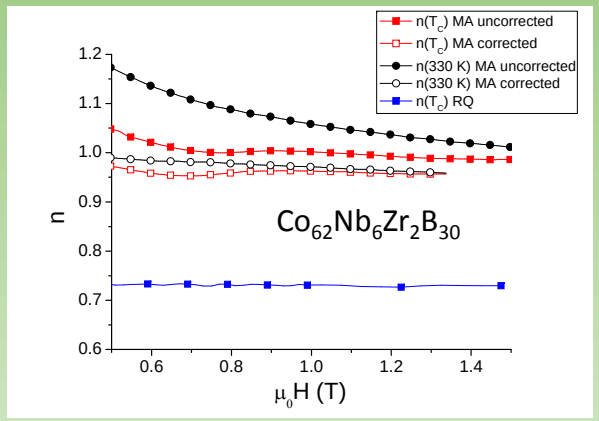

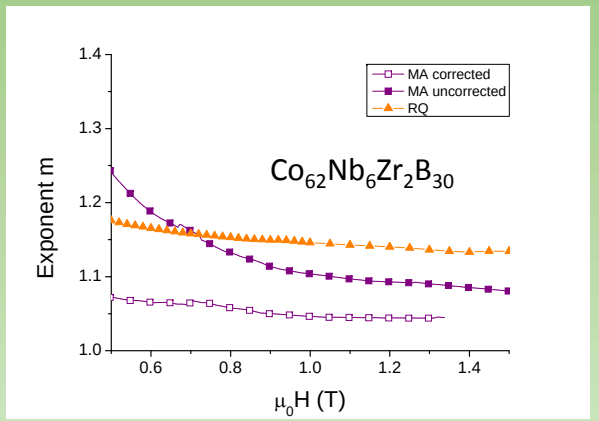

ΔS_m(T) and n(T) of rapidly quenched (RQ) alloy and mechanically alloyed (MA) samples uncorrected and corrected from N_D

Exponents n(Tc) and m for uncorrected and corrected ΔS_m curves

Moreno-Ramírez et al. J. All. Compd. 622(2015)606

Analysis of multiphase systems

- ✓Data corrected from demagnetizing field can be analyzed to extract information for individual phases

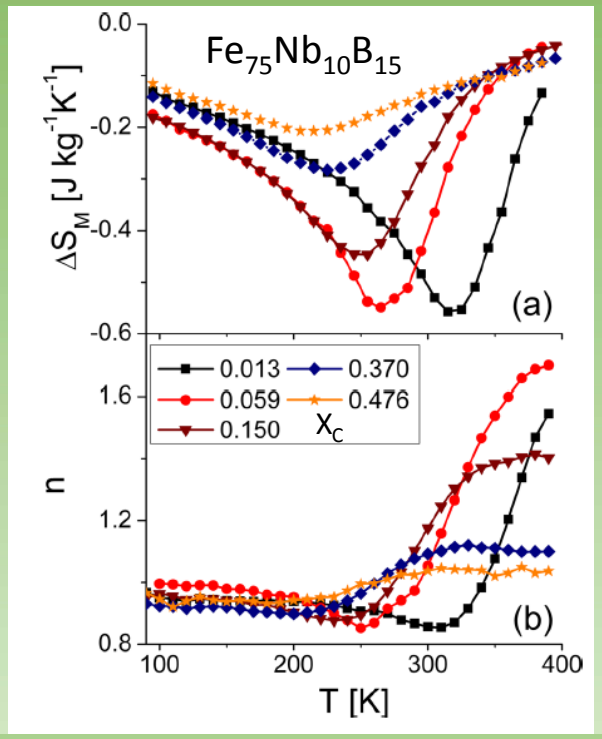

$\Delta S_m(T)$ and n(T) of mechanically alloyed samples corrected from N_D

$$\Delta S_m = a_c X H^{n_c} + a_A (1-X) H^{n_A}$$

$$n^{pk} = \frac{d \ln(\Delta S_m^{pk})}{d \ln(H)} = \frac{a_c n_c X H^{n_c} + a_A n_A (1-X) H^{n_A}}{\Delta S_m^{pk}}$$

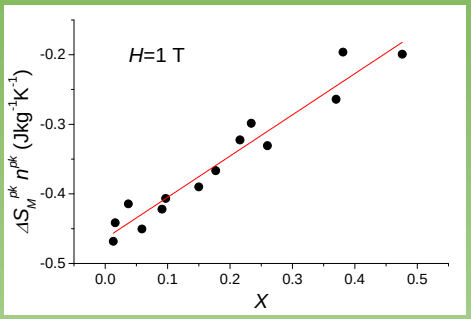

$$n^{pk} \Delta S_m^{pk} = \left(a_c n_c H^{n_c} - a_A n_A H^{n_A}\right) X + a_A n_A H^{n_A}$$

- ✓n_A independent on the technique used to measure X
- ✓Cancel the effect of impurity phases

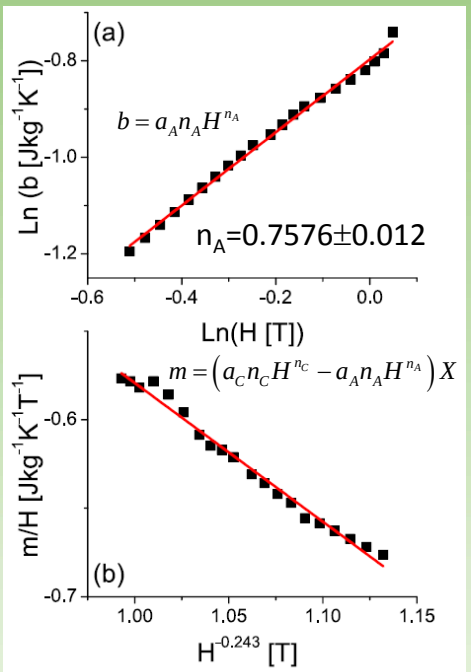

Ipus et al. Appl. Phys. Lett.105(2014)172405

Distribution of Curie temperatures

- ✓Broader MCE peaks are generally observed in milled samples with respect to quenched ones due to smearing of the transition
- ✓Ascribed to broader compositional distribution

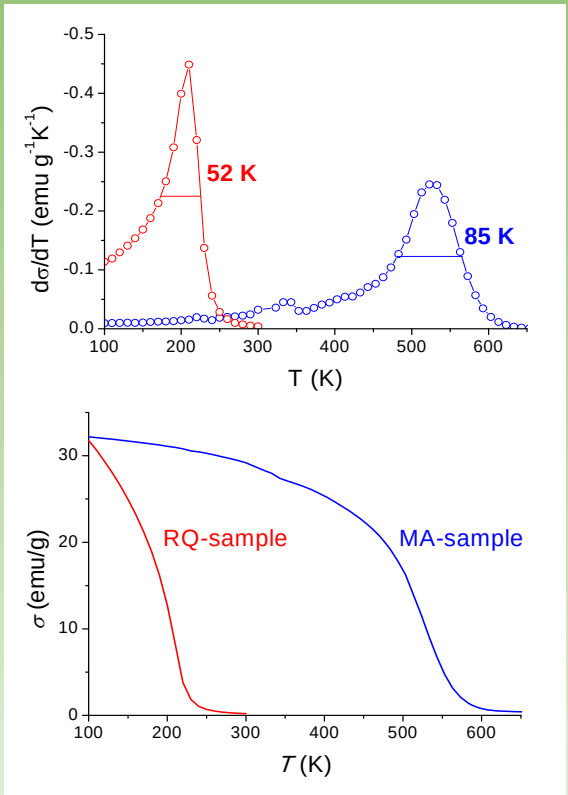

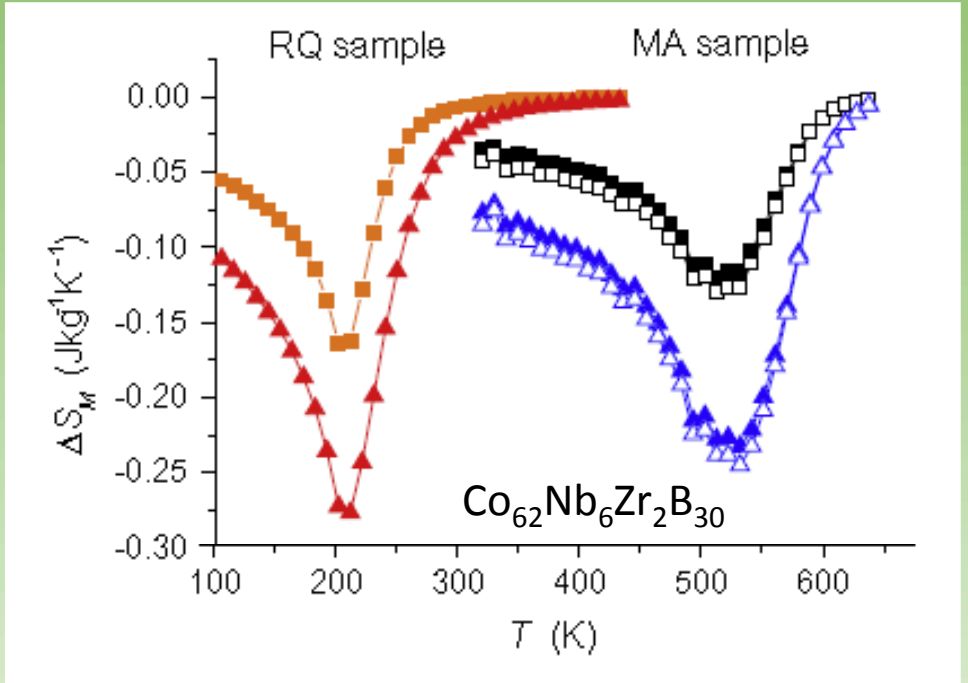

Moreno-Ramírez et al. J. All. Compd. 622(2015)606

- Experimental curves are fitted using Arrott-Noakes EOS

$$H^{1/\gamma} = a\left(T - T_C\right)M^{1/\gamma} + bM^{1/\gamma+1/\beta}$$

✓Melt-spun sample using a single curve using the critical exponents derived from Kouvel-Fisher method

✓Milled sample was fitted using a sum of curves with a distribution of T_C

$$\Delta S_m\left(T\right) = C\sum_{T_C^i = T_C - \Delta}^{T_C + \Delta} \Delta S_m\left(T, T_C^i\right) e^{-\frac{\left(T_C - T_C^i\right)^2}{2\sigma^2}}$$

✓Temperature dependence of n is described

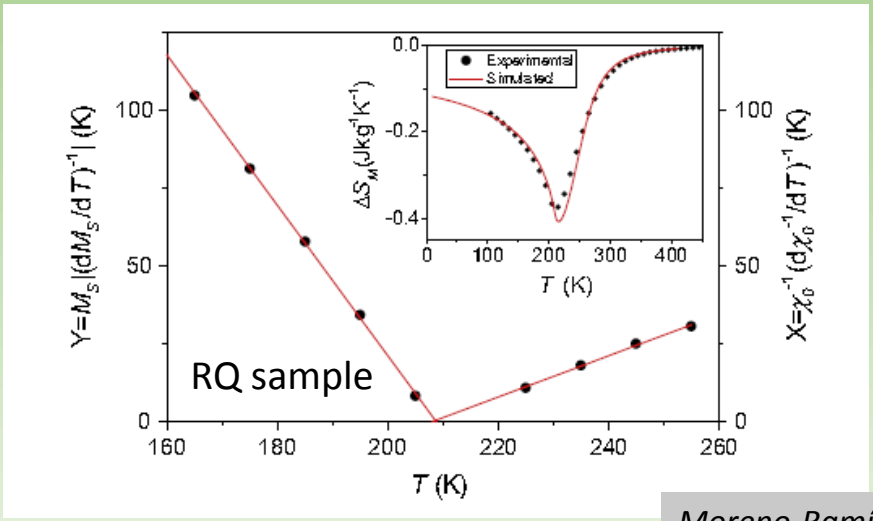

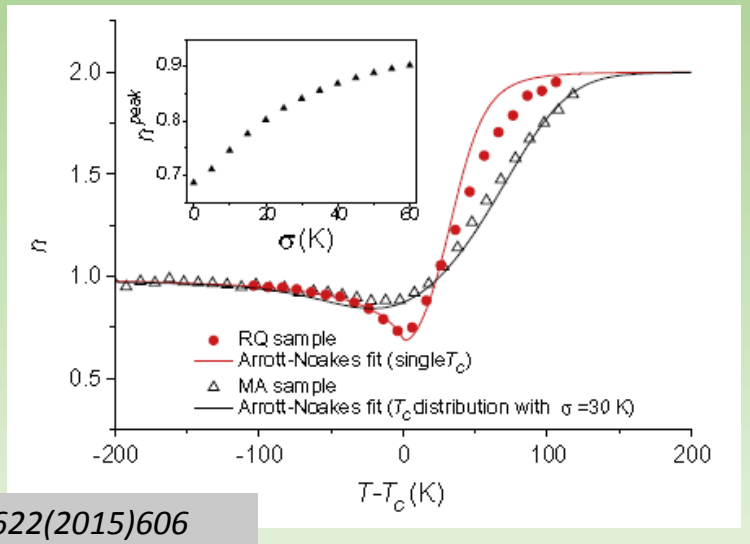

Moreno-Ramírez et al. J. All. Compd. 622(2015)606

MCE software developed

MCE Data Analysis program *V. Franco et al. Magn. Bus. Technol. 13 (Winter 2014) 8*

Available at www.lakeshore.com/products/Vibrating-Sample-Magnetometer/pages/MCE.aspx

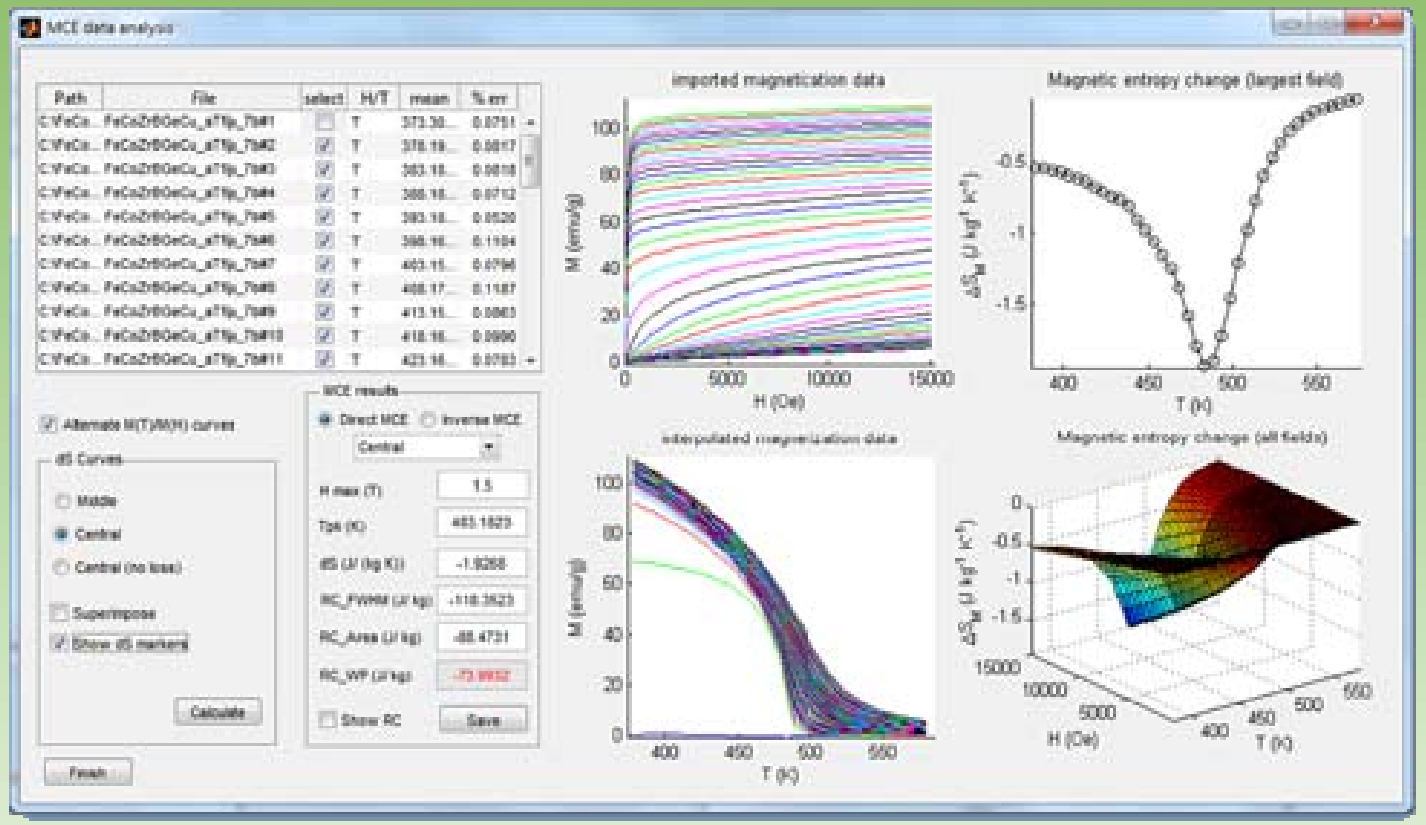

Conclusions

- Mechanical alloying, a succesful technique for metastable materials or prealloyed systems.
- Understanding dynamics to optimize process and to compare results from different labs.
- Composition of supersaturated solid solutions measured indirectly.
- Microstructure characterized by two size scales: powder particle size and crystal size.
- Two regimes affecting magnetic anisotropy evolution with milling time.
- Demagnetizing field affects MCE, particularly the field dependence of MCE parameters.
- Information from individual phases extracted from field dependence of MCE.
- Broadening and reduction of MCE of milled powder explained using a distribution of T_C.

Acknowledgments

- Spanish Ministry of Science and Innovation and EU FEDER (Projects MAT 2010-20537 and MAT 2013-45165-P),
- PAI of the Regional Government of Andalucía (Project P10-FQM-6462),
- United States Office of Naval Research (Project N00014-11-1-0311)

THANK YOU FOR YOUR ATTENTION!

Sevilla, December 11th 2015